11-2013

The Decomposition of Hydrazine in the Gas Phase and over an Iridium Catalyst

Michael Schmidt
Iowa State University, mike@si.fi.ameslab.gov

Mark S. Gordon
Iowa State University, mgordon@iastate.edu

The Decomposition of Hydrazine in the Gas Phase and over an Iridium Catalyst

Abstract
Hydrazine is an important rocket fuel, used as both a monopropellant and a bipropellant. This paper presents theoretical results to complement the extensive experimental studies of the gas phase and Ir catalyzed decompositions involved in the monopropellant applications of hydrazine. Gas phase electronic structure theory calculations that include electron correlation predict that numerous molecular and free radical reactions occur within the same energy range as the basic free radical pathways: NN bond breaking around 65 kcal/mol and NH bond breaking around 81 kcal/mol. The data suggest that a revision to existing kinetics modeling is desirable, based on the energetics and the new elementary steps reported herein. A supported Ir6 octahedron model for the Shell 405 Iridium catalyst used in thrusters was developed. Self-Consistent Field and electron correlation calculations (with core potentials and associated basis sets) find a rich chemistry for hydrazine on this catalyst model. The model catalyst provides dramatically lower NN and NH bond cleavage energies and an even smaller barrier to breaking the NH bond by NH2 abstractions. Thus, the low temperature decomposition over the catalyst is interpreted in terms of consecutive NH2 abstractions to produce ammonia and nitrogen. The higher temperature channel, which has hydrogen and nitrogen products, may be due to a mixture of two mechanisms. These two mechanisms are successive NH cleavages with surface H + H recombinations, and the same type of assisted H2 eliminations found to occur in the gas phase part of this study.

Keywords
Hydrazine, Gas Phase, Ir Catalyst, Quantum Chemistry

Disciplines
Chemistry

Comments
This article is from *Zeitschrift für Physikalische Chemie* 227 (2013): 1301, doi:10.1524/zpch.2013.0404. Posted with permission.

Z. Phys. Chem. **227** (2013) 1301–1336 / **DOI** 10.1524/zpch.2013.0404

The Decomposition of Hydrazine in the Gas Phase and over an Iridium Catalyst

By Michael W. Schmidt and Mark S. Gordon*

Department of Chemistry and Ames Laboratory, Iowa State University, Ames IA 50011, USA

(Received February 22, 2013; accepted in revised form April 2, 2013)
(Published online September 30, 2013)

Hydrazine / Gas Phase / Ir Catalyst / Quantum Chemistry

Hydrazine is an important rocket fuel, used as both a monopropellant and a bipropellant. This paper presents theoretical results to complement the extensive experimental studies of the gas phase and Ir catalyzed decompositions involved in the monopropellant applications of hydrazine. Gas phase electronic structure theory calculations that include electron correlation predict that numerous molecular and free radical reactions occur within the same energy range as the basic free radical pathways: NN bond breaking around 65 kcal/mol and NH bond breaking around 81 kcal/mol. The data suggest that a revision to existing kinetics modeling is desirable, based on the energetics and the new elementary steps reported herein. A supported Ir_6 octahedron model for the Shell 405 Iridium catalyst used in thrusters was developed. Self-Consistent Field and electron correlation calculations (with core potentials and associated basis sets) find a rich chemistry for hydrazine on this catalyst model. The model catalyst provides dramatically lower NN and NH bond cleavage energies and an even smaller barrier to breaking the NH bond by NH_2 abstractions. Thus, the low temperature decomposition over the catalyst is interpreted in terms of consecutive NH_2 abstractions to produce ammonia and nitrogen. The higher temperature channel, which has hydrogen and nitrogen products, may be due to a mixture of two mechanisms. These two mechanisms are successive NH cleavages with surface H + H recombinations, and the same type of assisted H_2 eliminations found to occur in the gas phase part of this study.

1. Introduction

The primary focus of this work is on the mechanism(s) for the decomposition of the hydrazine monopropellant to a mixture of H_2, N_2, and NH_3 both in the gas phase and over the Shell 405 catalyst. This catalyst, which consists of Ir metal particles deposited on γ-alumina, serves as the ignition source for rocket motors using hydrazine fuel. The hydrazine-based engine is a workhorse thruster, since N_2H_4 is a pumpable liquid which can be stored for decade-long space missions. No complicated mixing with oxidizers is needed, hydrazine decomposition is fairly energetic, and the catalyst provides simple hypergolic ignition [1]. Because of the importance of hydrazine, a great deal of experimental research on both gas phase and catalyzed decomposition rates was done during

* Corresponding author. E-mail: mark@si.msg.chem.iastate.edu

the 1960s heyday of rocket development. This information is captured in a two volume, 2000+ page opus by Schmidt [1]. The same thruster also burns methyl substituted hydrazine, which is not considered here. The use of hydrazine as a bipropellant with various oxidizers [1] is also not considered here. A number of the reactions considered below are also relevant to the Haber process for producing ammonia from N_2 and H_2, but the focus of the current report is on the decomposition reactions leading to small molecules.

The Shell 405 catalyst [2] was developed in the 1960s. This catalyst is formed by depositing Ir from solution onto a γ-alumina support, chosen due to its hardness and its stability under the overpressure of repeated ignitions. Fairly large coverage by Ir metal is achieved in Shell 405. Various other oxide supports are now known to be active, as is pure Ir. Other transition metals have also been shown to decompose hydrazine. Small Ir clusters show some activity towards hydrazine as well as other catalytic reactions. Both Ir_4 and Ir_6 particles on a model support are considered here.

This paper contains three parts, each using molecular quantum chemistry methods to complement the predominantly experimental information that is available. Section 2 presents new and mainly molecular mechanisms as well as the accepted free radical mechanisms for gas phase hydrazine decomposition. Section 3 develops some small models for the real world Ir catalyst. Finally, results are presented in Sect. 4 for various N_2H_4 decomposition reactions on the catalyst model. Each section contains references to previous research, the theoretical methods employed in that section, and results. An overall summary concludes the paper.

2. Gas phase decomposition of N_2H_4

The decomposition reaction at 983 K produces the following product ratio [1],

$$N_2H_4 \rightarrow 0.91NH_3 + 0.54N_2 + 0.64H_2.$$

The foregoing stoichiometry is conventionally considered to arise from two product channels:

$$N_2H_4 \rightarrow NH_3 + 1/2N_2 + 1/2H_2 \quad \Delta H^\circ(0\,\mathrm{K}) = -33.8\,\mathrm{kcal/mol}$$
$$N_2H_4 \rightarrow N_2 + 2H_2 \quad \Delta H^\circ(0\,\mathrm{K}) = -22.8\,\mathrm{kcal/mol}$$

It is known that the proportion of products found in the latter channel increases with temperature; at least, relatively less ammonia is produced [3]. The decomposition of liquid hydrazine is slow [1], and proceeds according to

$$N_2H_4 \rightarrow 4/3NH_3 + 1/3N_2 \quad \Delta H^\circ(0\,\mathrm{K}) = -37.5\,\mathrm{kcal/mol},$$

The foregoing thermochemical values are based on the NBS tables [4]. It is known [5] that the two bonds in hydrazine have the following dissociation energies,

$$N_2H_4 \rightarrow 2NH_2 \quad \mathrm{BDE} = \Delta H^\circ(0\,\mathrm{K}) = 57\text{–}66\,\mathrm{kcal/mol}$$
$$N_2H_4 \rightarrow H + N_2H_3 \quad \mathrm{BDE} = \Delta H^\circ(0\,\mathrm{K}) = 81\,\mathrm{kcal/mol}$$

The uncertainty in the first value is discussed below.

Schmidt [1] lists 41 experimental studies of hydrazine decomposition between 1930 and 1998, with the majority of the work published during the 1960s. He gives as the "textbook mechanism" the following reactions, which are taken from the 1965 study of Eberstein and Glassman [6]. The "textbook mechanism" is entirely free radical chemistry:

initiation: $X^* + N_2H_4 \rightarrow X + 2^2NH_2$

propagation: $N_2H_4 + {}^2NH_2 \rightarrow NH_3 + {}^2N_2H_3$

$N_2H_4 + {}^2H \rightarrow NH_3 + {}^2NH_2$

$^2N_2H_3 + X \rightarrow N_2 + H_2 + {}^2H + X$

branching: $^2N_2H_3 + X \rightarrow {}^3NH + {}^2NH_2 + X$

$N_2H_4 + {}^3NH \rightarrow {}^2NH_2 + {}^2N_2H_3$

termination: $2^2NH_2 \rightarrow N_2H_4$

$2^2N_2H_3 \rightarrow 2NH_3 + N_2$

$^2NH_2 + {}^2N_2H_3 \rightarrow NH_3 + N_2 + H_2$

$^2H + {}^2N_2H_3 \rightarrow N_2 + 2H_2$

deactivation: $^2N_2H_3^* + X \rightarrow {}^2N_2H_3 + X^*$

where X is any colliding species in the vapor. Spin multiplicities higher than singlet are shown for all species throughout this paper as pre-superscripts.

A recently published kinetic model of hydrazine flames [5] used a total of 51 reactions, each of which involves at least one free radical. This mechanism [5] proposed that the same initiation step (breaking the weakest bond) and the first propagation step shown above control the decomposition in dilute mixtures. The reaction $2^2NH_2 \rightarrow N_2H_2 + H_2$ is proposed to be important for the propagation speed of the flame.

In contrast to the extensive experimental literature, theoretical studies focused on the gas phase 2N/4H system are surprisingly rare. Of course, many of the species or reactions considered below have been considered individually, but no attempt is made to survey that work here. There are three recent studies that attempt to treat the 2N/4H reactive system globally. A ReaxFF study of N_2H_4 decomposition [7] finds a simultaneous appearance time for NH_2, N_2H_3, and molecular HNNH as the reaction initiates. Hwang and Mebel [8] (HM) used second order perturbation theory (MP2) saddle points to elucidate key steps in the Haber process, which includes reactions involving hydrazine itself, and, of course, its decomposition products. Asatrayan, Bozelli, *et al.* [9] (ABSSN) used coupled cluster-based methods to investigate hydrazine decomposition. Both HM and ABSSN identify the ylide-like species H_3NNH as an important intermediate that has not been included in the modeling of experimental kinetics measurements. In addition, HM report molecular chemistry in which H_2 removes two hydrogens, in the reaction $NNH_2 + H_2 \rightarrow N_2 + 2H_2$, through a five atom cyclic transition state. ABSSN reported a similar six atom cyclic transition state, again removing two hydrogens, namely *cis*-HN=NH + $H_2 \rightarrow N_2 + 2H_2$. These two studies suggest that additional quantum mechanical results for both radical and molecular elementary steps would be useful.

The gas phase decomposition of hydrogen has accordingly been reinvestigated. Most saddle points have been found using closed shell or spin-restricted open shell MP2 codes [10,11] with the aug-cc-pVDZ basis set [12]. Zero point energies are

obtained at the same level. Energies are obtained using the completely renormalized coupled cluster singles and doubles with perturbative triples theory called CR-CC(2,3), available in both closed shell [13] and spin-restricted open shell [14,15] forms. These final energy calculations used the larger basis set, namely aug-cc-pVTZ [12]. Some of the species possess unique electronic structures, so where appropriate multi-configurational methods [16] have been used, including 2nd order perturbation energy corrections [17]. These exceptions to the use of CR-CC(2,3)/aug-cc-pVTZ//MP2/aug-cc-pVDZ methods are indicated below. Of course, all stationary points were characterized as minima or saddle points by computation of hessians, and reaction mechanisms were confirmed by following the intrinsic reaction coordinates (IRC). All calculations have been carried out with the GAMESS (General Atomic and Molecular Electronic Structure System) electronic structure code [18,19], whose design goals include advanced open shell and multireference methods for the treatment of species that may require them.

Barrier heights for approximately 50 saddle points are listed in Table 1. An expanded version of this Table is given as supplemental material, including the total energy and zero point energy of all species, including the minima. An emphasis was placed on locating reactions involving molecular (closed shell) transition states and intermediates, in addition to the expected radical reactions, to complement the vast experimental data. Molecular saddle points allow pathways for 1,1- and 1,2-elimination of H_2 through 5-atom and 6-atom rings:

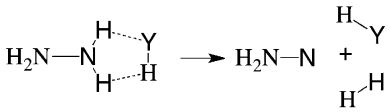

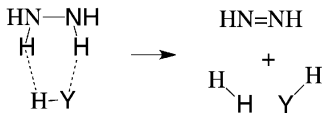

The "assisting" species HY (which is "catalytic" since it is regenerated) can be molecular hydrogen, ammonia, or hydrazine itself (Y=H, NH_2, N_2H_3). As will be seen, the saddle point structures for the foregoing reactions are with only one exception lower in energy than the 3-atom or 4-atom saddle point geometries for the direct elimination of H_2. As was noted above, HM [8] already included one example of an H_2-assisted 1,1-elimination from NNH_2, and ABSSN [9] gave one example for the H_2-assisted 1,2-elimination from *cis*-HN=NH.

Figure 1 summarizes the gas phase decomposition of hydrazine. Its four panels focus on (a) early steps in the process, (b) ^2H atom chemistry, (c) $^2NH_2$ and ^3NH free radical chemistry, and (d) molecular routes to products. Activation enthalpies and reaction enthalpies for individual reactions are given in Table 1.

The energy scale used in Fig. 1 attempts to place as much data as possible onto a 2N/4H energy scale. Following ABSSN [9], the zero of energy is set to the lowest

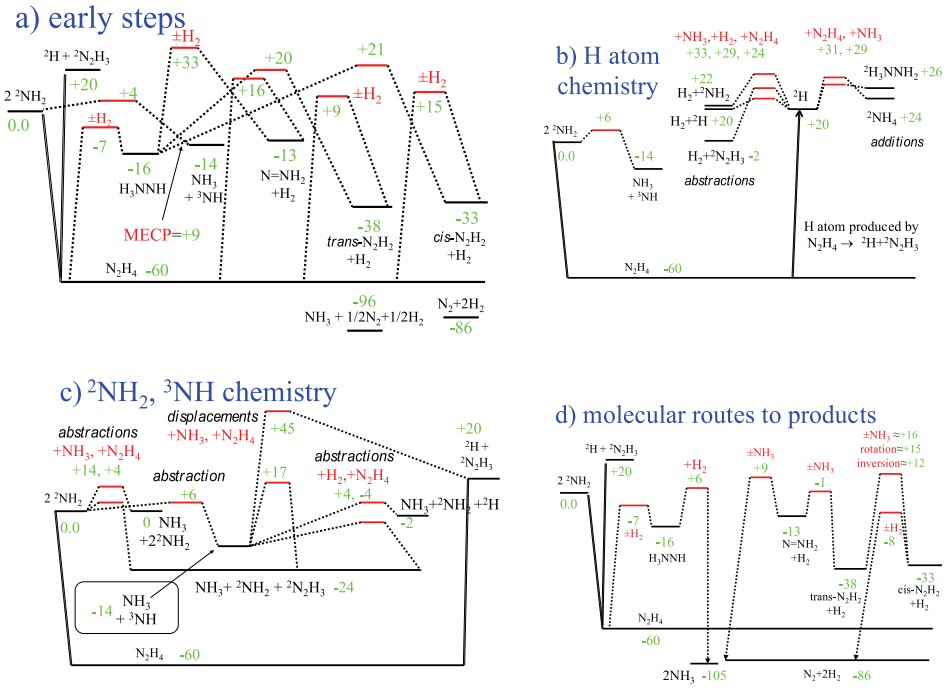

Fig. 1. Reaction enthalpies from CR-CC(2,3)/cc-pVTZ//MP2/cc-pVDZ, including zero point corrections. Shifted to a 2N/4H energy scale, with zero being $2\,^2NH_2$. Assisting species which come and go at the saddle are shown in red as ±Y, while species which add are shown as +X (increasing the atom count from 2N/4H). MECP = minimum energy crossing point. See text for further details, and Table 1 for the raw data behind this summary.

free radical channel, namely $2\,^2NH_2$. This allows energies reaching into the free radical regime to be easily identified, since these 2N/4H energies will be positive. The reactions for which HY serves as an assisting catalyst are rewritten (for example) from

$$N_2H_4 + HY \rightarrow \text{saddle point} \rightarrow HN{=}NH + H_2 + HY$$

to:

$$N_2H_4 \rightarrow \text{saddle point} - HY \rightarrow HN{=}NH + H_2.$$

by subtracting HY throughout, thus placing the reactant, saddle point, and product energies on a 2N/4H atom count scale. Any such saddle point with the energy of HY subtracted is identified in the figures as ±HY, to show the assisting molecule HY that comes and goes. Only the lowest barrier of this type is shown, to keep Fig. 1 from being cluttered, but all three "assisted" energies are given in Table 1 along with the corresponding unassisted direct elimination barriers. Other saddle points, which consume some species X, and which therefore add atoms to the 2N/4H count are also shown in Fig. 1, by writing +X at the saddle point. In this case, the energies

Table 1. Elementary steps in the gas phase decomposition of hydrazine[a].

	as written			on 2N/4H scale		
	$E^a(0°)$	$\Delta H_P°$ (0°)		$\Delta H_R°$ (0°)	$E^a(0°)$	$\Delta H_P°$ (0°)
saddle points for molecular chemistry						
1,1-H_2 eliminations:						
$N_2H_4 \leftrightarrow H_2 + NNH_2$	76.0	46.9	no shift	−60.0	16.0	−13.0
$H_2 + N_2H_4 \leftrightarrow 2H_2 + NNH_2$	97.9	46.9	$-H_2$	−60.0	37.9	−13.0
$H_3NNH \leftrightarrow H_2 +$ *cis*-HNNH	37.0	−16.2	no shift	−16.3	20.7	−32.6
$H_3NNH \leftrightarrow H_2 +$ *trans*-HNNH	36.4	−21.2	no shift	−16.3	20.0	−37.6
$H_2 + H_3NNH \leftrightarrow 2H_2 +$ *cis*-HNNH	53.1	−16.2	$-H_2$	−16.3	36.7	−32.6
$H_2 + H_3NNH \leftrightarrow 2H_2 +$ *trans*-HNNH	50.7	−21.2	$-H_2$	−16.3	34.3	−37.6
$NNH_2 \leftrightarrow H_2 + N_2$	51.7	−73.1	$+H_2$	−13.0	38.6	−86.1
$H_2 + NNH_2 \leftrightarrow 2H_2 + N_2$	27.9	−73.1	no shift	−13.0	14.9	−86.1
$NH_3 + NNH_2 \leftrightarrow NH_3 + H_2 + N_2$	22.5	−73.1	$+H_2$-NH_3	−13.0	9.4	−86.1
1,2-H_2 eliminations:						
$N_2H_4 \leftrightarrow H_2 +$ *cis*-HNNH (MCSP[b])	125.3	27.4	no shift	−60.0	65.4	−32.6
$N_2H_4 \leftrightarrow H_2 +$ *trans*-HNNH (MCSP[b])	122.1	22.4	no shift	−60.0	62.1	−37.6
$H_2 + N_2H_4 \leftrightarrow 2H_2 +$ *cis*-HNNH	75.0	27.4	$-H_2$	−60.0	15.0	−32.6
$H_2 + N_2H_4 \leftrightarrow 2H_2 +$ *trans*-HNNH	69.0	22.4	$-H_2$	−60.0	9.0	−37.6
$NH_3 + N_2H_4 \leftrightarrow NH_3 + H_2 +$ *cis*-HNNH	80.0	27.4	$-NH_3$	−60.0	20.0	−32.6
$NH_3 + N_2H_4 \leftrightarrow NH_3 + H_2 +$ *trans*-HNNH	77.3	22.4	$-NH_3$	−60.0	17.4	−37.6
$N_2H_4 + N_2H_4 \leftrightarrow N_2H_4 + H_2 +$ *cis*-HNNH	76.1	27.4	$-N_2H_4$	−60.0	16.1	−32.6
$N_2H_4 + N_2H_4 \leftrightarrow N_2H_4 + H_2 +$ *trans*-HNNH	75.5	22.4	$-N_2H_4$	−60.0	15.5	−37.6
$H_3NNH \leftrightarrow H_2 + NNH_2$	126.2	3.3	no shift	−16.3	109.9	−13.0
$H_2 + H_3NNH \leftrightarrow 2H_2 + NNH_2$ (SOSP[b])	48.9	3.3	$-H_2$	−16.3	32.6	−13.0
cis-HNNH $\leftrightarrow H_2 + N_2$	89.7	−53.6	$+H_2$	−32.6	57.2	−86.1
$H_2 +$ *cis*-HNNH $\leftrightarrow 2H_2 + N_2$	24.9	−53.6	no shift	−32.6	−7.6	−86.1
$NH_3 +$ *cis*-HNNH $\leftrightarrow NH_3 + H_2 + N_2$	32.8	−53.6	$+H_2$-NH_3	−32.6	0.3	−86.1
$N_2H_4 +$ *cis*-HNNH $\leftrightarrow N_2H_4 + H_2 + N_2$	31.9	−53.6	$+H_2$-N_2H_4	−32.6	−0.7	−86.1
isomerizations:						
$N_2H_4 \leftrightarrow H_3NNH$	93.1	43.6	no shift	−60.0	3.1	−16.3
$H_2 + N_2H_4 \leftrightarrow H_2 + H_3NNH$	52.5	43.6	$-H_2$	−60.0	−7.4	−16.3
$NNH_2 \leftrightarrow$ *cis*-HNNH	69.5	−19.5	$+H_2$	−13.0	56.4	−32.6
$NNH_2 \leftrightarrow$ *trans*-HNNH	46.9	−24.5	$+H_2$	−13.0	33.9	−37.6
$H_2 + NNH_2 \leftrightarrow H_2 +$ *trans*-HNNH	22.9	−24.5	no shift	−13.0	9.9	−37.6
$NH_3 + NNH_2 \leftrightarrow NH_3 +$ *trans*-HNNH	10.0	−24.5	$+H_2$-NH_3	−13.0	−0.6	−37.6
other reactions:						
$H_2 + H_3NNH \leftrightarrow 2NH_3$	22.1	−89.2	$-H_2$	−16.3	5.7	−105.5
trans-HNNH $\leftrightarrow$ *cis*-HNNH (inversion)	50.0	5.0	$+H_2$	−37.6	12.5	−32.6
trans-HNNH $\leftrightarrow$ *cis*-HNNH (rotation)	∼53[b]	5.0	$+H_2$	−37.6	∼15	−32.6
$NH_3 +$ *trans*-HNNH $\leftrightarrow NH_3 +$ *cis*-HNNH	53.6	5.0	$+H_2$-NH_3	−37.6	16.0	−32.6
$N_2 + N_2H_4 \leftrightarrow 2$ *cis*-HNNH	80.1	81.0	$-N_2$	−60.0	20.1	21.0

can still always be shifted to lie on the same 2N/4H scale. An example is shown in panel b, where the "as written" 13.2 kcal/mol barrier and 1.7 kcal/mol endothermicity for $^2H + NH_3 \rightarrow H_2 + {}^2NH_2$ are repositioned to start at +20.1 kcal/mol, which is the energy required to produce H atoms by NH cleavage of hydrazine. To be specific,

$$^2H + NH_3 \rightarrow \text{ saddle } \rightarrow H_2 + {}^2NH_2$$

Table 1. Continued.

	as written $E^a(0°)$	$\Delta H_P°$ (0°)		on 2N/4H scale $\Delta H_R°$ (0°)	$E^a(0°)$	$\Delta H_P°$ (0°)
saddle points for radical chemistry						
cleavages:						
$N_2H_4 \leftrightarrow 2\,^2NH_2$	n/a	60.0	no shift	−60.0	n/a	0.0
$N_2H_4 \leftrightarrow {}^2H + {}^2N_2H_3$	n/a	80.1	no shift	−60.0	n/a	20.1
abstractions:						
$^2H + H_2 \leftrightarrow H_2 + {}^2H$	8.9	0	$+{}^2N_2H_3$-H_2	20.1	29.0	20.1
$^2H + NH_3 \leftrightarrow H_2 + {}^2NH_2$	13.2	1.7	$+{}^2N_2H_3$-NH_3	20.1	33.3	21.8
$^2H + {}^2N_2H_3 \leftrightarrow H_2 +$ *cis*-HNNH	≤3[b]	−52.7	no shift	20.1	≤23	−32.6
$^2H + {}^2N_2H_3 \leftrightarrow H_2 +$ *trans*-HNNH	≤1[b]	−57.7	no shift	20.1	≤21	−37.6
$^2H + {}^2N_2H_3 \leftrightarrow H_2 + {}^3NNH_2$	2.2	−33.1	no shift	20.1	22.3	−13.6
$^2H + {}^2N_2H_3 \leftrightarrow H_2 + {}^3HNNH$	9.4	−15.8	no shift	20.1	29.5	4.3
$^2H + N_2H_4 \leftrightarrow H_2 + {}^2N_2H_3$	4.1	−22.1	$+{}^2N_2H_3$-N_2H_4	20.1	24.1	−2.0
$^3NH + H_2 \leftrightarrow {}^2NH_2 + {}^2H$	17.8	12.3	$+NH_3$-H_2	−14.0	3.8	−1.7
$^3NH + NH_3 \leftrightarrow 2\,^2NH_2$	19.9	14.0	no shift	−14.0	5.9	0.0
$^3NH + N_2H_4 \leftrightarrow {}^2NH_2 + {}^2N_2H_3$	9.6	−9.8	$+{}^2NH_3$-N_2H_4	−14.0	−4.4	−23.8
$^2NH_2 + NH_3 \leftrightarrow NH_3 + {}^2NH_2$	13.6	0	$+{}^2NH_2$-NH_3	0.0	13.6	0.0
$^2NH_2 + {}^2N_2H_3 \leftrightarrow NH_3 + {}^3NNH_2$	−1.2	−34.8	$+{}^2NH_2$-N_2H_3	0.0	−1.0	−34.8
$^2NH_2 + N_2H_4 \leftrightarrow NH_3 + {}^2N_2H_3$	3.6	−23.8	$+{}^2NH_2$-N_2H_4	0.0	3.6	−23.8
$^2N_2H_3 + N_2H_4 \leftrightarrow N_2H_4 + {}^2N_2H_3$	17.3	0	$-N_2H_3$	−60.0	−42.6	−60.0
displacements:						
$^3NH + NH_3 \leftrightarrow {}^2N_2H_3 + {}^2H$	59.4	34.1	no shift	−14.0	45.4	20.1
$^3NH + N_2H_4 \leftrightarrow {}^2N_2H_3 + {}^2NH_2$	30.6	−9.8	$+NH_3$-N_2H_4	−14.0	16.6	−23.8
additions:						
$^2H + NH_3 \leftrightarrow {}^2NH_4$	10.7	3.6	$+{}^2N_2H_3$-NH_3	20.1	30.8	23.7
$^2H + N_2H_4 \leftrightarrow {}^2H_3NNH_2$	9.1	6.0	$+{}^2N_2H_3$-N_2H_4	20.1	29.2	26.0
$^2H + N_2 \leftrightarrow {}^2NNH$	15.1	7.5	$+{}^2N_2H_3$-N_2	20.1	35.2	27.6

[a] Energy values (in kcal/mol) using CR-CC(2,3)/aug-cc-pVTZ//MP2/aug-cc-pVDZ energies combined with unscaled MP2/aug-cc-pVDZ zero point vibrational energies. The first two columns are the activation energies and exothermicities, for the reactions *exactly as written*, for which the enthalpy of reactants is zero. Figure 1 displays many of these shifted to a common overall 2N/4H energy scale, by adding or subtracting the indicated species from the reactants, saddle point, and products. After shifting, the final three columns are the energy of these three, relative to a zero of energy for $2\,^2NH_2$. Superscripts indicate the multiplicity of any species which is not a singlet.

[b] See text, regarding the use of one MCSCF rotational barrier, two MCSCF saddle point (MCSP) geometries, one MCSCF second order saddle point (SOSP), and two MCSCF constrained reaction pathways, instead of MP2.

is shifted by adding $^2N_2H_3$ and subtracting NH_3 throughout,

$$^2H + {}^2N_2H_3 \rightarrow \text{saddle} + {}^2N_2H_3{-}NH_3 \rightarrow H_2 + {}^2NH_2 + {}^2N_2H_3{-}NH_3$$

so that reactants, transition state, and products lie at 20.1, 33.3, and 21.8 kcal/mol, respectively, on the 2N/4H energy scale. The available space for labeling in Fig. 1b does not permit showing the shifting species, so this saddle is labeled as simply $+NH_3$, at the shifted energy +33 kcal/mol.

Figure 1 contains only energies shifted onto the 2N/4H scale, with zero set to $2\,^2NH_2$, as just described. In some places in the text, it is convenient to mention barri-

ers for a reaction exactly as it is written. Any energy in the text which is not labeled "as written" can be presumed to have been shifted to the 2N/4H scale. Both "as written" as well as 2N/4H shifted enthalpies for each individual reaction are given in Table 1. Zero point vibrational energies can be sizeable in this system, and are included in the relative energies in Fig. 1, so that Fig. 1 shows activation enthalpies and reaction enthalpies at 0 K.

Panel a of Fig. 1 shows energies for some important free radicals and molecular species, which might plausibly be involved in the decomposition of hydrazine. The accuracy of the present computational method for these key species should be assessed. The NBS tables [4] place the $NH_3 + 1/2N_2 + 1/2H_2$ and $N_2 + 2H_2$ channels 34 and 23 kcal/mol, respectively, lower in energy than N_2H_4. These experimental data are reproduced to within 3 kcal/mol by the computations presented herein: 36 and 26 kcal/mol, respectively, below N_2H_4. The heat of formation of *trans*-HN=NH is $\leq$ 48.8 kcal/mol [20], corresponding to a 0 K enthalpy of 26.0 kcal/mol for H_2+ HNNH relative to N_2H_4, so the value calculated here of 22 kcal/mol reproduces this experimental result to within 4 kcal/mol. CCSD(T)/aug-pV5Z enthalpy calculations [21] place *cis*-HN=NH 5.2 kcal/mol, and NNH_2 24.1 kcal/mol above *trans*-HN=NH compared to the 5 and 25 kcal/mol computed in the present work. For radical channels, the hydrazine NN and NH bond breaking reactions to $2\,^2NH_2$ and $^2H + {}^2N_2H_3$ are reproduced to similar accuracy. Note that the majority of NN bond dissociation energies cited by Konnov and de Ruyck [5] cluster around 60 kcal/mol, while a recent and perhaps most reliable experiment is 65.5 kcal/mol [22], with the present work obtaining 60.0 kcal/mol. Any underestimation of the energy requirement for the NN cleavage by a few kcal/mol will have implications for the degree of involvement of molecular chemistry as a direct competitor for free radical mechanisms, as will be seen below. The NH bond energy [5] of 81 kcal/mol is reproduced closely here, at 80.1 kcal/mol. The reader should regard this higher energy radical channel, $^2H + {}^2N_2H_3$, computed as +20.1 kcal/mol relative to the 2N/4H energy zero at $2\,^2NH_2$, to be an informal cutoff for "low energy processes". Both free radical and molecular routes to products will be demonstrated to exist below this +20 kcal/mol threshold. The calibrations in this paragraph suggest that the present high level gas phase results are accurate to 5 kcal/mol or better.

Representative gas phase saddle point structures are shown in Fig. 2. Only a subset of the more than 50 saddle point energies presented in Table 1 are shown in the Figure in order to conserve space.

Two consecutive 1,1-H_2 or two consecutive 1,2-H_2 eliminations will decompose hydrazine into the observed products $2H_2 + N_2$. Both routes have high barriers: the first and second 1,1-H_2 eliminations lie 16.0 and 38.6 kcal/mol above $2\,^2NH_2$, respectively, while the first and second 1,2-H_2 eliminations lie 62.1 and 57.2 kcal/mol above $2\,^2NH_2$. The first 1,2-H_2 elimination saddle point (Fig. 2a) has appreciable multireference character, so its energy is assessed by coupled cluster energies using MCSCF rather than MP2 saddle points [23]. Perhaps surprisingly, the 5-atom saddle point for H_2-assisted 1,1-H_2 elimination is 37.9 kcal/mol, higher than the unassisted 1,1-H_2 saddle at 16 kcal/mol. Therefore, the H_2 assisted 1,2-H_2 elimination discussed next is energetically preferred over any type of 1,1-H_2 pathway. The initial 1,2-H_2 elimination energy requirement of 62.1 kcal/mol beyond $2\,^2NH_2$ is dramatically reduced to 9.0,

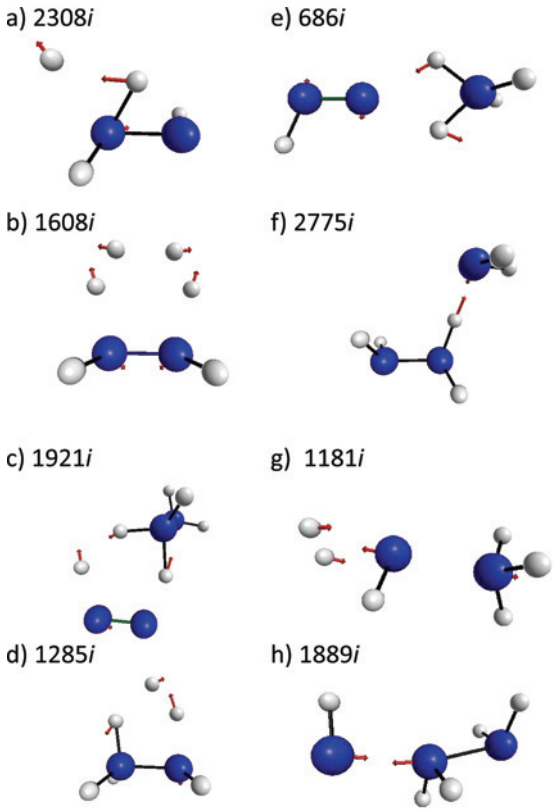

Fig. 2. Representative MP2 gas phase transition states, with their corresponding imaginary frequencies: a) 1,2-H_2 elimination from hydrazine, by MCSCF rather than MP2. b) H_2-assisted 1,2-H_2 elimination. c) hydrazine-assisted 1,2-H_2 elimination from *cis*-HNNH. d) H_2-assisted isomerization of hydrazine to activated hydrazine. e) NH_3-assisted isomerization of *cis*- to *trans*-HNNH. f) NH_2 abstraction of H from hydrazine. g) H_2 reaction with activated hydrazine, producing $2NH_3$ h) S_n2-like attack of ^3NH on hydrazine, displacing $^2NH_2$.

17.4, or 15.5 kcal/mol by reactions with assisting H_2 (Fig. 2b), NH_3, or N_2H_4 species, respectively. The second 1,2-H_2 elimination barrier is also greatly reduced, as discussed below.

ABSNN [9] refer to the ylide-like H_3NNH species as "activated hydrazine". It is accessible by a direct isomerization through a 3-atom saddle [9] at an activation energy of +3.1 kcal/mol, but the H_2-assisted 5-atom saddle point structure shown in Fig. 2d allows this species to be accessed *below* the threshold for any free radical process, at −7.4 kcal/mol on the 2N/4H scale in Fig. 1. Other molecules NNH_2 or *cis* or *trans* HNNH may then be reached from H_3NNH. The path to NNH_2 (isodiazene [24,25]) by direct 1,2-H_2 elimination is very difficult (∼110 kcal/mol), while the H_2-assisted path through a second order saddle point at 32.6 kcal/mol [26] is too high to compete with free radical chemistry, and also is less favorable than 1,1-elimimination from hydrazine. 1,1-H_2 eliminations with H_2 assistance require 20.0 or 20.7 kcal/mol to reach

trans or *cis*-HNNH, so these are also more easily accessed from hydrazine itself, rather than from "activated hydrazine". Finally, ABSNN pointed out that by spin-inversion at a minimum energy crossing point (MECP), the product species NH_3 along with a triplet state of NH can be reached from "activated hydrazine". The present results show an energy for this MECP [27] (+9 kcal/mol; Fig. 1) that is higher than the straightforward abstraction of a hydrogen by one NH_2 from another, namely 5.9 kcal/mol. The true importance of "activated hydrazine" is discussed later.

Panel b of Fig. 1 shows part of the free radical chemistry, involving H atoms. On the left are repeated the low energy pathways to the radicals $^2NH_2$ and ^3NH, whose chemistry is in panel c. The right side of Fig. 1b shows that H atoms are able to perform abstraction reactions, giving the decomposition product H_2. However, these barriers are necessarily above the 20 kcal/mol informal definition of "low energy pathways" since H atom is generated by a $+20.1$ kcal/mol channel hydrazine $\rightarrow {}^2H + {}^2N_2H_3$. (See also, Table 1). Of course, H atoms may recombine with any other free radical. Such radical recombinations are assumed to occur with no barrier, for example the recombination $^2H + {}^2NH_2 \rightarrow NH_3$. On the other hand, the H atom can add to N-species, by approaching a lone pair, with the unpaired electron winding up in a diffuse orbital. For example, $^2NH_3NH_2$ can be viewed as closed shell cation $NH_3NH_2^+$ neutralized by an electron in a large orbital. These kinds of species may in fact open up ion chemistry, as this diffuse electron might be easily detached by collisions in a hydrazine flame. Ions are not considered further here.

Panel c of Fig. 1 shows the chemistry of $^2NH_2$ and ^3NH. Much of this panel has labeling with atom counts different from 2N/4H, but the barriers and energies are all shifted to the common 2N/4H scale. For example, the "as written" 9.6 kcal/mol barrier for the abstraction reaction $^3NH + N_2H_4 \rightarrow {}^2N_2H_3 + {}^2NH_2$ appears at -4.4, when shifted to the -14.0 kcal/mol 2N/4H species $^3NH + NH_3$. $^2NH_2$ may abstract H atoms from the closed shell species NH_3 or hydrazine (Fig. 2f), shown at the left of Fig. 1c, through barriers which remain in the low energy range. In fact, the reaction of $^2NH_2$ with hydrazine requires only $+3.6$ kcal/mol to produce an $^2N_2H_3$ radical. This 3.6 kcal/mol barrier is well below the +20 kcal/mol $^2N_2H_3$-producing channel shown at the far right of Fig. 1c. ^3NH is located at the center of panel c, easily reached by the $^2NH_2 + {}^2NH_2$ self-abstraction [28]. The reverse of this $+5.9$ kcal/mol reaction is the abstraction reaction for ^3NH from NH_3. The ^3NH abstractions from H_2 or hydrazine are shown to the right of ^3NH in panel c. All three ^3NH abstraction barriers are low, including a -4.4 kcal/mol saddle point that also leads to the two radicals $^2NH_2 + {}^2N_2H_3$. Just to the right of ^3NH are two higher energy (+45.4, $+16.6$ kcal/mol) displacement reactions, which in carbon chemistry terms, might be called S_N2 mechanisms. The lower energy displacement saddle point structure at $+16.6$ kcal/mol is the reaction of imidogen with the hydrazine fuel, and is shown in Fig. 2h.

Free radical chemistry easily explains the products H_2 or NH_3, which can be formed via the abstraction reactions discussed above, or by the presumably barrierless recombinations of $^2H/{}^2H$ and $^2H/{}^2NH_2$. It is not so easy to see how free radicals lead to the third observed product, N_2. The textbook mechanism quoted at the start of this section involves termination steps in which the ^2H (or $^2NH_2$) abstractions from $^2N_2H_3$ are assumed to proceed directly to final products H_2 (or NH_3) $+ N_2 + H_2$. An MP2 saddle point was readily found for ^2H attack at either the NH or the NH_2 end of $^2N_2H_3$ on

the overall triplet surface, with modest "as written" barriers after coupled cluster energy evaluation and the incorporation of zero point effects: +2.2 and +9.4 kcal/mol, respectively. Similarly the triplet coupled attack of $^2NH_2$ at the NH end of $^2N_2H_3$ has an "as written" barrier which falls below the reactants after coupled cluster and ZPE corrections, to −1.2 kcal/mol. However, the reaction paths from these saddle points lead to products H_2 (or NH_3) and either ^{3}HNNH or $^3NNH_2$; that is, the latter triplet species do not fall completely apart to $H_2 + N_2$. After a spin conversion, ^{3}HNNH or $^3NNH_2$ could reach the N_2 product by the molecular processes discussed below. On the slightly higher energy singlet-coupled $^2H + {}^2N_2H_3$ surface, around the saddle point regions on the triplet surface, there are two orbitals with occupation numbers close to 1 in the full valence MCSCF (all valence orbitals and electrons active) wavefunction. Accordingly, the termination reaction $^2H + {}^2N_2H_3$ was considered using full valence MCSCF calculations, so that any reactive channel is possible, including the assumption in the textbook mechanism that the reaction leads directly to N_2 and $2H_2$. However, no saddle point could be located on these singlet surfaces. Therefore, pathways were constructed at various fixed HH distances with nearly linear HHN geometries, for the attack of ^2H on each of two possible target hydrogen atoms at the NH_2 end of $^2N_2H_3$. Optimization of all other geometry parameters except the HH distance and HHN angle gave pathways that connect $^2H + {}^2N_2H_3$ with H_2 and either *cis*-HNNH or *trans*-HNNH. The maximum energy anywhere along these pathways is barely higher than the reacting $^2H + {}^2N_2H_3$: 3 kcal/mol and 1 kcal/mol for the ^2H attacks producing *cis*-HNNH and *trans*-HNNH, respectively. Saddle point searches begun at these small maxima proceeded towards the reactants $^2H + {}^2N_2H_3$ at large separations. It is likely that there is no barrier to these abstractions on the singlet surfaces, but these two upper limits on the "as written" barriers are listed in Table 1. It is important to note that, as was the case for triplet reaction paths, the constrained pathways on the singlet surface $^2H + {}^2N_2H_3$ do not lead to $2H_2 + N_2$ as implied by the "textbook mechanism". The final panel of Fig. 1 shows how N_2 is actually produced.

Panel d of Fig. 1 returns to molecular pathways, showing how H_3NNH or the three species NNH_2 and *trans*- or *cis*-HN=NH reach the final products: H_2, N_2, and NH_3. Both HM[8] and ABSNN[9] have discovered the saddle point for the reaction of "activated hydrazine" with hydrogen: $H_3NNH + H_2 \rightarrow 2NH_3$. This reaction has an overall barrier of +5.7 kcal/mol, competitive with the lowest +5.9 kcal/mol NH_3-producing channel reported in the free radical processes discussed above. The saddle is shown in Fig. 2g. This reaction is, by far, the most important involving "activated hydrazine".

The 6-atom cyclic transition state for the H_2-assisted dehydrogenation of *cis*-HN=NH was discovered by ABSNN, and this low energy saddle became the inspiration for the effort in the present work to locate many more molecular reactions. The similar 6-atom cyclic transition state for the hydrazine-assisted dehydrogenation of *cis*-HN=NH is shown in Fig. 2c. The H_2-assisted reaction appears facile at −7.6 kcal/mol, but note that to reach *cis*-HN=NH requires either the +15.0 kcal/mol H_2-assisted dehydrogenation of hydrazine in Fig. 1a, or the +9.0 kcal/mol H_2-assisted dehydrogenation to reach *trans*-HN=NH followed by a +12.5 kcal/mol inversion barrier [29] from the *trans* isomer. In other words, the three partially dehydrogenated intermediates NNH_2 and *trans*- or *cis*-HN=NH can fully interconvert in the scheme shown in Fig. 1d at a cost of +12.5 kcal/mol, and are most easily reached by a +9.0 kcal/mol

process to *trans*-HN=NH shown in Fig. 1a. Thus molecular chemistry involving these three species occurs about halfway in energy between the 0 kcal/mol NN cleavage to the radical pair $^2NH_2$ and the +20 kcal/mol NH cleavage to radicals $^2H + {}^2N_2H_3$. The +9 to +12 kcal/mol energy requirements for the group of reactions at the right side of Fig. 1d, when compared to the +5.7 kcal/mol energy requirement at the left of panel d, or the +5.9 kcal/mol radical pathway to ammonia discussed above, offers a simple possible explanation for the experimental observation [3] that N_2/H_2 product formation increases relative to NH_3 products as the temperature increases.

Some final comments about energies [21,30] for HN=NH and NNH_2 are appropriate. First, an obvious alternate for *cis*/*trans* interconversion besides inversion is a rotation about the N=N double bond. As this completely breaks a π bond, it requires an MCSCF treatment. In order to include electron correlation in the calculation, the four-electrons in four orbitals (4,4) MCSCF calculation was followed by a second order multi-reference perturbation theory (MRMP2) calculation. The non-zero point corrected MCSCF/aug-cc-pVTZ and MRMP/aug-cc-pVTZ "as written" rotational barriers are 65 and 53 kcal/mol above *trans*-HN=NH. The former is very close to the previously published value [31] of 65 kcal/mol using MCSCF/3-21G. The 53 kcal/mol MRMP2 barrier in the present work is also close to the previous estimate of 55 ± 6 [28]. After conversion to the 2N/4H energy scale of Fig. 1, the internal rotation corresponds to a non-ZPE corrected MRMP2 barrier of $\approx +15$ kcal/mol. Another *cis*/*trans* interconversion involves a 4-atom NH_3-assisted cyclic saddle, shown in Fig. 2e, whose +16.0 kcal/mol energy also lies just above inversion. Thus, H_2-assisted dehydrogenation of hydrazine (+9.0 kcal/mol) to *trans*-HN=NH followed by inversion to *cis* (+12.5 kcal/mol) affords a slightly lower pathway to *cis*-HNNH than the H_2-assisted dehydrogenation directly to *cis* (+15.0 kcal/mol). Note that the +12.5 kcal/mol inversion barrier need not be surmounted for all three 2N/2H species to reach products, as the +9.4 kcal/mol NH_3-assisted dehydrogenation of NNH_2 shown in Fig. 1d accomplishes that at a slightly lower energy. (NNH_2 is the only species for which NH_3 or N_2H_4-assisted saddles, which are typically very similar to each other in both energy and geometry, are lower than H_2-assisted reactions).

Molecular routes are competitive with the free radical chemistry widely assumed to be the only player (*e. g.*, the "textbook mechanism" or the more elaborate kinetics model of reference 5). For example, two completely molecular pathways within the 0–20 kcal/mol energy range in which numerous free radical reactions also occur are:

(a) An H_2-assisted isomerization of N_2H_4 to "activated hydrazine", followed by a reaction with H_2 to produce $2NH_3$ has a maximum energy requirement of 5.7 kcal/mol,

(b) The H_2-assisted dehydrogenation of N_2H_4 to *trans*-HNNH, followed by NH_3-assisted isomerization to NNH_2, followed by NH_3-assisted dehydrogenation, to overall products $N_2 + 2H_2$, has a maximum energy requirement of 9.4 kcal/mol.

3. Catalyst models

In the rocket thruster of interest, the Shell 405 catalyst consists of 30 weight percent dispersed crystallites of Ir on γ-alumina, with particle sizes about 2 nm as determined by electron diffraction [32]. TEM images are also available, showing similar sized crystal-

lite Ir particles [33]. Ir/Al_2O_3 materials with Ir weight 5% to 20% prepared by alternate techniques to the Shell 405 preparation have been studied by X-ray diffraction and TEM [34,35], suggesting these samples may contain Ir_xO_y. It is also known that Ir shows catalytic behavior for hydrazine (as well as other species such as hydrocarbons) in many other environments. These include polycrystalline or (111) Ir surfaces [36–39], as well as Ir particles supported on carbon nanofibers [40], MgO [41,42], or zeolites [43,44]. It should also be noted that hydrazine decomposition can occur over other metals, such as rhodium [45], rhodium on alumina [46], Mo_2N on γ-alumina [47], NbN_xO_y [48] and iron on MgO [49]. Reactivity of course depends on the reacting species, the metal, its particle size, and the support, with Shell 405 being particularly effective for hydrazine decomposition.

Size controlled clusters of Ir are of particular interest. Clusters from Ir_{18} to Ir_{39} on Ir(111) have been studied [50], finding a preference for planar hexagonal shapes. The Gates group has performed extensive experiments using carbonyl precursors such as $Ir_4(CO)_{12}$ [51] and $Ir_6(CO)_{16}$ [52], with review articles available [53,54]. Flow treatment by H_2 removes all carbonyls, leaving a bare Ir_4 or Ir_6 cluster on γ-alumina. XAFS for these clusters [42,55,56] shows a single value for the IrIr distance, about 2.67 Å, with an IrIr coordination number of about 3; two distinct IrO distances around 2.05 and 2.7 Å, with a coordination number around 1 for the close contact [42]; and in one report, tentative IrAl distances are given [56]. This structural information is consistent with preservation of the original tetrahedral Ir_4 or octahedral Ir_6 cores. Reactivity towards ethene hydrogenation is found to be slightly larger for Ir_4 than for Ir_6 [56], and to be larger on alumina than MgO supports [42]. Experiments with an Ir_8 carbonyl precursor (consisting of two Ir_4 tetrahedra) were found to retain two Ir_4 particles on γ-alumina [57]. Very similar results are found by the Gates group for Ir_n on zeolites [43,44,59,60] where treatment by ethene is found to generate atomic Ir_1 species [44,59,60], but treatment by H_2 regenerates Ir_4, whose further treatment by CO will regenerate the original adsorbed Ir_4 carbonyls. Alternatively, the Anderson group sputtered Ir_n^+ to form Ir_n/Al_2O_3 film/NiAl(110), up to $n = 15$, and observed hydrazine decomposition [61,62]. Their observations show that decomposition rates increase with cluster size, particularly from $n = 7$; however no information is available about their Ir_n cluster shapes. Basini and coworkers [63] have studied Ir_n on α-alumina, again using the carbonyl precursor $Ir_4(CO)_{12}$ and treatment with He/H_2 to decarbonylate. Their higher temperature conditions (500 °C) lead to aggregates Ir_x of unknown size, with coordination numbers ranging from 4.5 to 10.8 and IrIr distances around 2.70 Å: these are likely to be three dimensional metallic crystallites. No Ir/α-alumina structural information is given [63]. Taken together, these studies indicate that small Ir clusters are anchored on the supports, show catalytic activity towards hydrazine and also other species, with reactivity tending to increase with cluster size. The present work considers supported Ir_4 and Ir_6 clusters, with more emphasis on the latter.

There has been some theoretical work involving unsupported (naked) Ir clusters. Two density functional theory (DFT) studies on bare Ir_n clusters for $n = 4, 6, 8, 10$ [64] and $n = 2$–15 [65] have been published. Both studies find singlet Ir_4 to be a tetrahedron, while singlet Ir_6 is a prism. Both studies find isomers of lower symmetry for higher spin multiplicities, with energies close to the singlets. Without giving any details, the SCF plus MP2 methodology described below gives similar results: SCF level energies

are lowest for higher multiplicities, but including correlation energy by MP2 favors the high symmetry closed shells. The prism geometry for bare Ir_6 is not the relevant one, as demonstrated below, the anchored Ir_6 prefers an octahedral geometry over the prism. Thus catalytic modeling studies should be performed using a realistic model for the support. However, there is a theoretical study of the reactions of H_2 with a bare Ir_4 cluster [66,67].

The support used for Shell 405 is γ-alumina, which is a hard material capable of withstanding initiation overpressure during repeated thruster firings. This ceramic material is a commonly used catalyst support [68], whose bulk and surface structures are not well understood [69], as indicated by the brief sampling of the literature which follows. There is one report of a single crystal structure [70]. The bulk structure type is usually described as a spinel defect, but the location of its cation vacancies is now known to be considerably more complicated [71] and the real-world material may include hydrogen [72] or foreign ions [73]. γ-Alumina surfaces exhibit long range disorder [74,75]. The chemical nature of the surface is controversial, in part due to the possibility of water absorption leading to surface hydroxyls [72,75] (*i. e.*, the details of the γ-alumina surface probably depend on its exposure history) and there is conflicting information about the existence of surface Al atoms [76]. There is some modeling work for γ-alumina, including a MD simulation of the surface structure [77], band structure for the bulk [78],and studies of hydroxyl [75], water [79] or metal oxides [80] such as CuO adsorbed on the surface.

α-Alumina (known as ruby or corundum after low levels of Cr doping) is another common support material, including Ir_n particles [63], which are known to be active on a wide variety of supports including alumina films (see above). All the alumina phases interconvert [81]. α-alumina has a definite composition Al_2O_3, and well-known ordered structures, both in the bulk [82] and for its cleavage surface [83]. α-Alumina consists of planes of O atoms between layers of Al atoms, as one moves in the z-direction (normal to the cleavage plane). Atoms in the Al layer alternate their z coordinate slightly, so that half are closer to one O plane, and half to the other. Cleavage of the (0001) surface occurs between these two half-layers of Al. The surface reconstructs by drawing its half-layer of aluminum nearly into the first O layer, with more subtle layer spacing changes below this. A recent simulation [84] in excellent agreement with experiment gives a good overview of the (0001) reconstructed surface. The top layer of this surface contains some triangular oxygen sites with an aluminum atom present in the center and other triangular oxygen sites with aluminum atoms one layer below. Either trio of oxygen atoms affords a location for interaction with a triangular face of Ir_4 or Ir_6.

Due to the large system size when catalytic models are used, the theoretical methodology in the present section (which is also used in Sect. 4), is necessarily more approximate than could be used for the gas phase hydrazine results presented in Sect. 2 above. The 6-31G(d) basis set is used for the H, N, O, Si, Al atoms [85–89], while the relativistic SBKJC effective core potential and basis set is used for Ir [89]: both sets are used in spherical harmonic form. Minima were found using closed or spin-restricted open shell SCF [90], with correlation energies estimated by closed or open shell MP2 [10,11]. All calculations employ the package GAMESS [18]. Some idea of the accuracy of the SCF/SBKJC&6-31G(d) geometries can be gleaned from

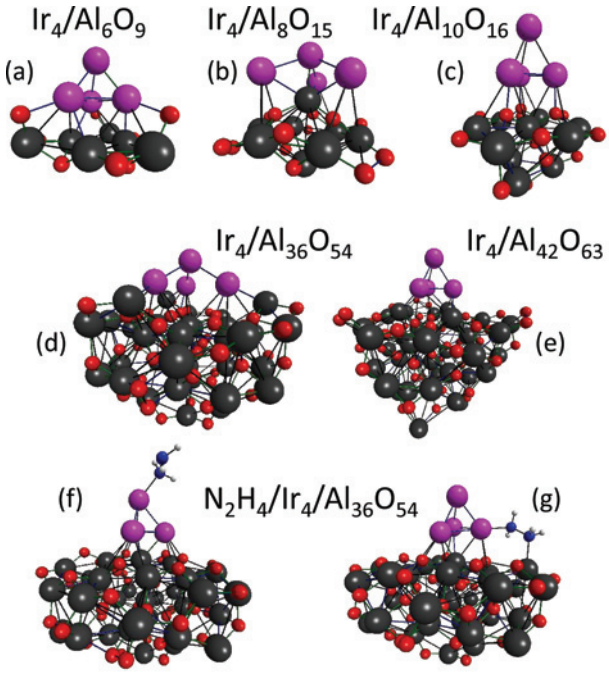

Fig. 3. Top row: two distorted small slabs [(a),(b)], and a small symmetrical slab (c) that distorts in the presence of N_xH_y species. Middle: O_3Al-centered open Ir_4 (d) and O_3-centered tetrahedral Ir_4 (e) (both isomers exist on both slabs). Bottom: N→Ir coordination with IrIr edge elongation (f), and a surface interaction (g), both for the tetrahedral O_3Al-centered slab. Color code: Ir: purple, Al: black, O: red, N: blue, H: white.

$Ir_4(CO)_{12}$. The structural predictions are IrIr = 2.704 Å, IrC = 1.964 Å, CO = 1.120 Å, compared to the X-ray structure values IrIr = 2.693, IrC = 1.87, and assumed CO = 1.14 Å [51].

Ir_x/alumina slab structures are shown in Fig. 3. These were prepared by extracting atom positions from the crystal structure of α-alumina [82] with compositions as close as possible to the stoichiometry Al_2O_3. Some small models were created by hand. Slabs include Al_6O_9, Al_8O_{15}, $Al_{10}O_{16}$, $Al_{20}O_{30}$, $Al_{36}O_{54}$, and $Al_{42}O_{63}$. Geometry optimization with small slabs often rearrange the attached Ir_4 particle or the alumina slab, or both. Figure 3 shows that Al_6O_9 rearranges to have unphysical IrAl contacts, with three O atoms rising up around the Ir_4 particle, while for Al_8O_{15} the Ir_4 opens at its base and an Al atom intrudes. Both are in disagreement with the experimental observations reported by Gates et al [56], which indicate intact metal tetrahedra and short IrO surface contacts. $Ir_4Al_{10}O_{16}$ successfully produces a correct Al/O layered structure with 3-fold symmetry and the desired IrO surface contacts; unfortunately, geometry optimizations with added N_xH_y species result in the $Al_{10}O_{16}$ slab deforming into globular shapes and/or partial detachment of the Ir_4. The additional atoms in $Al_{20}O_{30}$ impart more rigidity, but this slab (based on a bulk cut of $Al_3O_{12}Al_{10}O_{12}Al_7O_6$) is still somewhat deformable.

Three-fold symmetric $Al_{36}O_{54}$ and $Al_{42}O_{63}$ slabs based on bulk cuts with layer compositions $Al_7O_{21}Al_{12}O_{18}Al_{13}O_{12}Al_4O_3$ and $Al_6O_{21}Al_{13}O_{24}Al_{13}O_{12}Al_7O_6Al_3$ respectively are the most successful slabs. These are now large enough to possess overall rigidity. $Al_{36}O_{54}$ has an Al-containing O_3 triangle at its center, while $Al_{42}O_{63}$ has an open site O_3 center (with an Al atom one plane below). Depending on the geometry optimization protocol (pre-optimize the bare slab before adding and fully optimizing Ir_x on the slab, *versus* adding Ir_x to crystal structure coordinates prior to full optimization), two different minima were found for each type of centering, with one of each type shown in Fig. 3. In one structure type, Fig. 3e, the Ir_4 tetrahedron is intact, sits above the surface, and each Ir is connected to one O atom: this is in agreement with the limited structural information reported by the Gates group [56]. In the other structure type, Fig. 3d, the bottom Ir triangle opens up to IrIr distances about 4.0 Å with both IrO and IrAl contacts. Both types of structures have 3-fold symmetry, and are positive definite minima at the SCF level. The opened form is more stable at the SCF level, by 9(21) kcal/mol for $Al_{36}O_{54}$ ($Al_{42}O_{63}$). Considering the large system size and the lack of correlation energy treatment, these tetrahedral and open forms should be regarded as possessing "similar" energies. Probe calculations with Ir_6 on $Al_{36}O_{54}$ found similar octahedral and open isomers. The local malleability of alumina underneath Ir_4 is not surprising in view of the need to use very large slabs to gain overall rigidity. Structural details of the interactions between surface particles and supports are often unclear, but chemistry at these interfaces should not be surprising. For example: experiments using Pd nanoparticles show sintering converts transition alumina (γ,θ,δ) into α-alumina [91,92], experiments for Pt nanoparticles on γ-alumina find hydrogen between the metal and alumina prior to high temperature treatment [93], and modeling studies of Cr atoms on γ-alumina indicate that Cr prefers to move into a subsurface site [94].

Figure 3 shows selected results for the adsorption of hydrazine on $Ir_4/Al_{36}O_{54}$. Nine geometry optimizations with hydrazine positioned slightly away from the Ir_4 were started, varying in whether H or N atoms were pointing towards the metal, and varying in location: above, at edges, or at faces. Most searches terminated with one nitrogen lone pair directed to the unique apical Ir atom, sometimes with pronounced tilting of the Ir/alumina attachment, or as in the less modified structure shown in Fig. 3f, at least elongation of an IrIr edge. Figure 3g shows one interesting possibility occurring on large slabs: the hydrazine is coordinated to one of the bottom metals and also is coordinated to the surface. None of these trials resulted in hydrazine decomposition, or H to Ir attachment, but only N to Ir attachments, differing in the Ir sites and in internal rotations within the hydrazine.

While it is possible to create a catalyst model with Ir_4 or Ir_6 on α-alumina slabs, the satisfactory slabs are impractically large to carry out all of the numerous minima or saddle point searches that are relevant for the decomposition of hydrazine. Petrova, Rösch, and coworkers have used twelve-membered rings with three-fold symmetry: c-[-SiH_2-O-AlH_2-O-]$_3^{-3}$ balanced by three Na^+ ions [95] or the hydroxyl containing c-[-Si(OH)H-OH-Al(OH)H-O-]$_3$, which is neutralized by O protonation [96–99], as models for zeolite supports of Ir_4. The lower energy structure of the former model [95] binds three Ir atoms to three oxygens. The hydroxyl groups in the latter model [96–99] surround but do not bond to the three attached Ir atoms. Reactions with various numbers

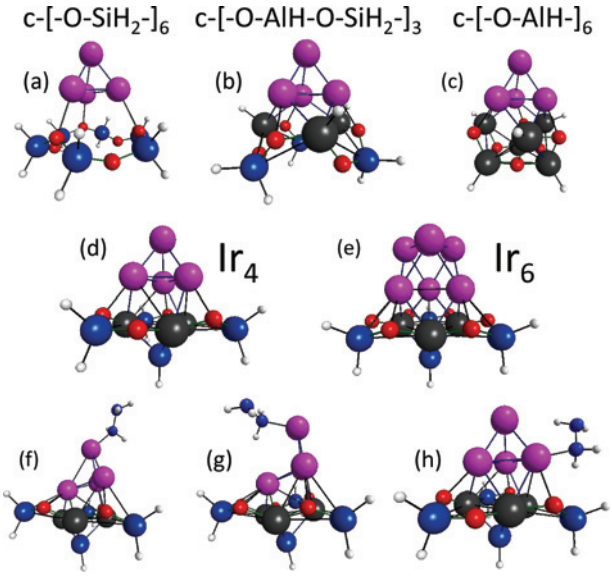

Fig. 4. Top: Ir_4 on Si (a), mixed Al/Si (b), and Al-containing (c) twelve atom open rings ((c) is rearranged upon geometry optimization). The middle and bottom rows are supported on the tethered c-[-O-Al-O-SiH2-]$_3$SiH. Middle: Ir_4 and Ir_6 particles. Bottom: some representative N_2H_4 interactions with the Ir_4 model of the middle row. Color codes as in Fig. 3; Si support atoms are dark blue.

of H_2 molecules were studied [96–99]. A study of 3 H atoms on a similar Ir_6/zeolite model is available [100].

The small rings designed by Rösch and co-workers were the inspiration for the catalyst model used here, after some adaptation, such as elimination of the hydroxyls. Open rings with twelve heavy atoms such as c-[-O-AlH-]$_6$, c-[-O-AlH-O-SiH$_2$-]$_3$, and c-[-O-SiH$_2$-]$_6$ were considered, by placing the atoms of the bottom triangle of Ir_4 (see, for example, Fig. 4) above one oxygen, or between two oxygens, generating six trial structures. The terminology "open ring" means that there is no tethering atom present at the center of the ring, so these rings look like one large open circle. The top row of Fig. 4 shows the three results for these six attempts. All six possibilities conserve the Ir_4 tetrahedron. Ir_4 floats off the Si-containing rings, to a long distance of IrO $\sim$ 2.60 Å; of course this model is also unsatisfactory in that it has no aluminum. The Al-containing rings deform extensively under geometry optimization, often to close IrAl contacts, which is not surprising in view of the distortions described above for small alumina slabs. The mixed Al/Si rings are more satisfactory: the ring distorts in a way that places the SiH_2 far from the metal, with each Ir near two Al and one O atoms. Structures constrained by 3-fold C_{3v} symmetry to have two IrO contacts have imaginary frequencies, which are eliminated by rotating the Ir_4 until there is only one close IrO contact, hence there are only three minima shown in the top row of Fig. 4. The final catalyst model was created by adding a SiH "tether" at the bottom of the mixed Al/Si system, bonded to the Al atoms, namely c-[-O-Al-O-SiH$_2$-]$_3$SiH.

The final Ir_4 tethered model, Fig. 4d, has a roughly planar Al/O "surface", each Ir has one IrO contact, as well as an IrAl contact, and its side SiH_2 groups are well away from the Ir. Figure 4e shows that octahedral Ir_6 has a similar structure. Since the gas phase singlet Ir_6 structure is a prism, the initial Ir_6 model was prepared as a prism, with its two triangular faces directly above each other. This C_{3v} symmetric geometry has a small imaginary frequency, and geometry optimization in this a_2 direction results in an energy lowering of about 10 kcal/mol, as the top triangle of Ir rotates so as to be opposed to the lower triangle. The optimization recovers C_{3v} symmetry, with the same octahedral Ir_6 core found in the $Ir_6(CO)_{18}$ precursor structure. Note that the Ir_4 species optimizes to one close IrO and one long IrO contact, while Ir_6 contains two equal IrO distances. Let Ir^b denote the three bottom Ir atoms, which are attached to the support model, while Ir^t means the top one or three Ir atoms. Key distances in the RHF/SBKJC/6-31G(d) structure of Ir_4/c-[-O-Al-O-SiH_2-]$_3$SiH are $Ir^tIr^b = 2.48$ Å, $Ir^bIr^b = 2.57$ Å, $Ir^bO = 2.27$ Å and 3.27 Å, and $Ir^bAl = 2.66$ and 3.19 Å. For Ir_6/c-[-O-Al-O-SiH_2-]$_3$SiH the important distances are $Ir^tIr^t = 2.52$ Å, $Ir^tIr^b = 2.65$ Å and 3.78 Å, $Ir^bIr^b = 2.90$ Å, two $Ir^bO = 2.27$ Å, and two $Ir^bAl = 2.62$ Å. These may be compared to XAFS data [56] for Ir_6 on γ-alumina: IrIr ~ 2.63 Å and ~ 3.73 Å (the latter is the diameter of the octahedron), IrO ~ 2.07 Å with coordination number just below one, IrAl ~ 2.43 Å again with coordination number less than one. The Ir^bSi distances in the models are quite long: 3.21 Å in the Ir_4 model and 2.81 Å for Ir_6. Note that the bottom SiH tether and the side SiH_2 groups are both essential for the rigidity of the catalyst model, while Ir still interacts only with Al and O atoms.

Before considering the rigidity of these models under hydrazine attack, it is useful to address their spin multiplicity. The singlet state of the Ir_4/model (where model = c-[-O-Al-O-SiH_2-]$_3$SiH) possesses C_3 symmetry. Geometry optimization on the triplet and quintet states distort slightly to C_1 symmetry. At the SCF level, the energy ordering is singlet 0.0, triplet −22, and quintet −31 kcal/mol. However, electron correlation introduced with MP2 reverses this: the singlet at energy 0.0 is substantially more stable than triplet +56 and quintet +76 kcal/mol. A similar reversal of the SCF stability order by MP2 correlation energies was found for bare tetrahedral Ir_4 and prism Ir_6, as noted above. All calculations in the next section treat the catalyst model as being in the singlet state.

Nine trial structures for the attack of hydrazine on the Ir_4/model were generated by rotating N_2H_4 around its x, y, z directions, and placing each orientation around the top, edge, or face of the catalyst. The N_2H_4 remained intact after all optimizations. Five trials resulted in the coordination of one N lone pair above the apical Ir, one trial led to this same coordination mode at a bottom Ir, and the remaining three trials opened one IrIr edge with N coordination at the now two-coordinate apical Ir. Figure 4 shows typical structures. Notice that hydrazine also induces changes in the Ir_4/model contact interactions, such as tipping of the Ir_4 and elongation of some IrO distances. The edge-opening instability of the Ir_4 structure is consistent with experimental findings that treatment of Ir_4/zeolite by ethylene generates surface Ir_1/ethylene species [44]. Opening the edges of the tetrahedral Ir_4 cluster is undoubtedly an important part of its chemistry. The metal octahedron in the Ir_6/model is more robust when exposed to hydrazine or other N_xH_y species. The octahedron can distort, and on rare occasion rearrange, but no edge openings occurred. Since the Ir_6 model has three atoms on its top surface, it affords a greater

number of reaction possibilities, such as transfer of hydrazine fragments to an adjacent Ir site. Accordingly, the following section considers hydrazine decomposition upon the tethered catalyst model Ir_6/c-[-O-Al-O-SiH_2-]$_3$SiH.

4. Hydrazine decomposition on a model catalyst

Extensive experimental studies for the kinetics of hydrazine decomposition over the Shell 405 catalyst (or similar materials) exist, and are reviewed in Schmidt's book [1]. Some fundamental studies [38,101], more recent experiments [33–35], and thruster kinetic modeling [102,103] should be noted.

Two theoretical studies of the details of hydrazine decomposition exist, both involving a metal surface, rather than a supported metal particle. The computational technique in both studies is plane wave DFT simulations with periodic boundary conditions. The study on Fe(211) [104] carried out unimolecular NH cleavages, with barriers about 1 eV, stepping all the way to N_2 plus H atoms. The NN cleavage of each N_2H_y species was found to be slightly more facile than its NH cleavages. NH_3 product could be rationalized by NH_2 picking up a surface H atom, with no discussion of H_2 production. The study on Ir(111) [105] also considered sequential NH cleavages, as well as the initiating NN cleavage to produce two NH_2 groups. The abstraction reactions of the latter from N_2H_y species were found to be important.

To set the scene for the following discussion, recall that

a) The overall stoichiometry is three products often formally written as two channels: $N_2 + 2H_2$ and $NH_3 + 1/2N_2 + 1/2H_2$, particularly in the gas phase. More precisely, experiments [101] for Ir on alumina catalysts show that below 300 °C products arise almost exclusively from $3N_2H_4 \rightarrow 4NH_3 + N_2$, while above 600 °C the reaction has stoichiometry $N_2H_4 \rightarrow N_2 + 2H_2$. Intermediate temperatures show both channels.

b) The experimental NN and NH bond strengths of hydrazine are 65 and 81 kcal/mol, respectively.

c) Molecular and radical channels exist within this same 65–81 kcal/mol energy range in the gas phase.

d) The model for the supported catalyst is Ir_6/c-[-O-Al-O-SiH_2-]$_3$SiH, which has an octahedral Ir_6, three surface Ir atoms for multi-site chemistry, only IrO and IrAl close contacts, and gains rigidity through its Si groups. It is referred to below as Ir_6/model.

4A. Methods. The computational method is similar to that used in Sect. 3: p functions are added to hydrogen, because of their presence in the reacting hydrazine, making the basis set 6-31G(d,p)&SBKJC [85–89]. Spin-restricted SCF wavefunctions were used to find geometries, saddle points, and reaction paths. Hessians were always computed to characterize stationary points as being minima or saddles. Reaction mechanisms were verified by following the SCF level intrinsic reaction coordinate [106] (IRC) from saddles to their adjacent minima. Energies for all species are presented using closed or spin-restricted open shell MP2 [10,11]. For singlets, a parallel CCSD(T) program [107] could be used to check the MP2 results. CCSD(T) energies, where available, are given in parentheses after the MP2 energies. The energies given in this section do not contain zero point corrections.

4B. Structures and energies. Although the Ir_6/model is fairly rigid, geometry optimizations and transition state searches sometimes result in distortions, most commonly, detachment of an Ir from its base, especially when there is unpaired electron character in the bottom Ir layer. The Ir_6 octahedron is more robust than the tetrahedron, with opening of IrIr sides or rearrangement to Ir_4Ir_2 layers both being fairly rare. Insertion of radicals such as H or NH_2 into an IrIr top edge is found to occur. Whenever a distorted structure was found, the geometry of the reacting N_xH_y species was copied onto a clean Ir_6/model, and reoptimized. This frequently resulted in a less distorted structure, allowing the original distorted geometry to be ignored. However, stretching of IrO bonds is common, so sometimes one or two of the six IrO bonds present in the Ir_6/model are elongated. The plus sign notation N_2H_4+ Ir_6/model means hydrazine is in the gas phase, while writing N_2H_4/Ir_6/model means hydrazine is adsorbed onto the catalyst. Since the Ir_6 particle has three top atoms, it may sometimes adsorb species at all three sites, for example, $NH_2/N_2H_4/Ir_6$/model. A total of about 150 N_xH_y minima and about 80 saddle points have been located. Only the most relevant reaction pathways are discussed below.

Energies in this section and the related figures are presented wherever possible relative to the MP2 (or CCSD(T), in parenthesis) energy of $N_2H_4(g) + Ir_6$/model, which is chosen as 0.0 kcal/mol. Where necessary, the same procedures to keep energies on a 2N/4H scale as discussed above for the gas phase decomposition are used. For example, the hydrogen assisted reaction $H_2 + N_2H_4/Ir_6$/model $\rightarrow$ N_2H_6/Ir_6/model $\rightarrow$ $2H_2$+ HNNH/Ir_6/model is rewritten by subtracting the energy of H_2 from all sides: N_2H_4/Ir_6/model $\rightarrow$ N_2H_6/Ir_6/model -H_2 $\rightarrow$ H_2+ HNNH/Ir_6/model. When it is interesting to consider the barrier for a single step, comparing the energy of some intermediate to the corresponding reaction barrier height, this is termed the "direct path" or "direct barrier", to distinguish these from energies shifted to the common 2N/4H scale.

4C. Electronic structure of surface radicals. Figure 5 shows the singly occupied molecular orbital for doublet spin surface species NH_2, H, and N_2H_3. NH_2 retains some unpaired electron character on the nitrogen atom, but this orbital also extends onto the Ir. An H atom on the surface results in an unpaired d electron on the Ir atom to which it is attached; interestingly, other H surface isomers can have their unpaired d electrons on an adjacent top Ir atom (not shown). N_2H_3 illustrates a case in which the unpaired electron sits at an Ir atom in the bottom layer. The final image in Fig. 5 is from singlet H + H. Orbital number 97 at orbital energy $\varepsilon = -0.58$ h is an orbital with appreciable hydridic character. This orbital lies well below the highest occupied molecular orbital (HOMO: orbital 127, with $\varepsilon = -0.28$ h)! The ability of the Ir_6 cluster to at least partially quench surface radical character results in stabilization of surface radicals, and when two "radicals" are present, the Ir-cluster creates a tendency for singlet coupling of these. The singlet H + H isomer (one of several) shown in Fig. 5 lies 29 kcal/mol below a high spin triplet coupling of the surface H + H, based on MP2 energies. Similarly, when two NH_2 radicals are attached at adjacent corners, the MP2 energy preference for a closed shell singlet is 39 kcal/mol over the triplet coupling. The implications for catalysis are obvious: iridium stabilizes surface "radicals" by partly or fully quenching their open shell character, and creates a preference for singlet chemistry.

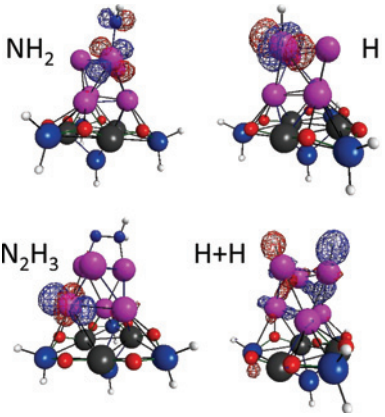

Fig. 5. Singly occupied MO of some adsorbed radicals: NH_2 shows appreciable delocalization into the adjacent top Ir, H shows complete transfer of the radical center onto a top Ir, and N_2H_3 places its odd electron on a bottom Ir atom. One H+H orbital φ_{97} with hydridic character is shown, this filled orbital lies far below the HOMO φ_{127}. Atom color code as in Fig. 4.

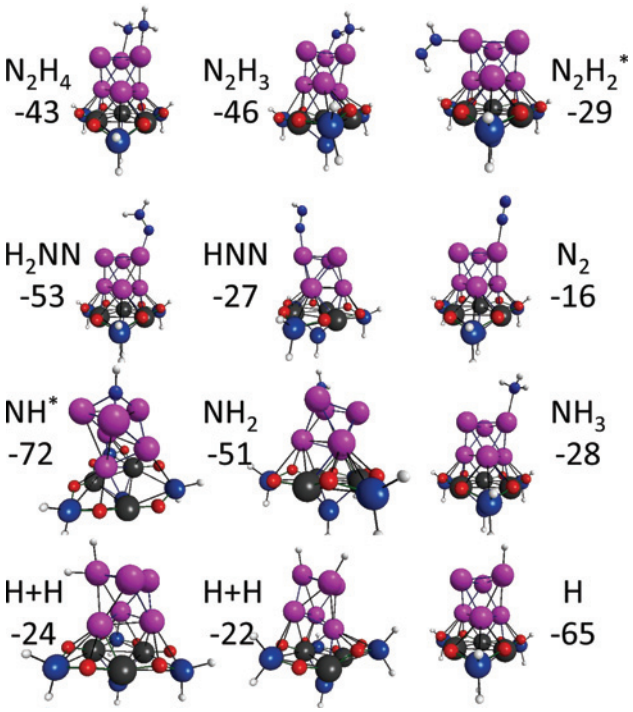

Fig. 6. Typical adsorbed N_2H_y species. Values give the MP2 level adsorption energies, in kcal/mol, for the lowest energy isomer. Stars mark two interesting isomers which are not the lowest energy. The lowest energy for adsorbed NH is for the triplet (−72), while the face-coordinated isomer shown is a singlet. Note that adsorption can occur at the side (N_2H_2), with distortion of the Ir_6 octahedral (H), or with loss of a few IrO contacts (NH_2). Atom color code as in Fig. 4.

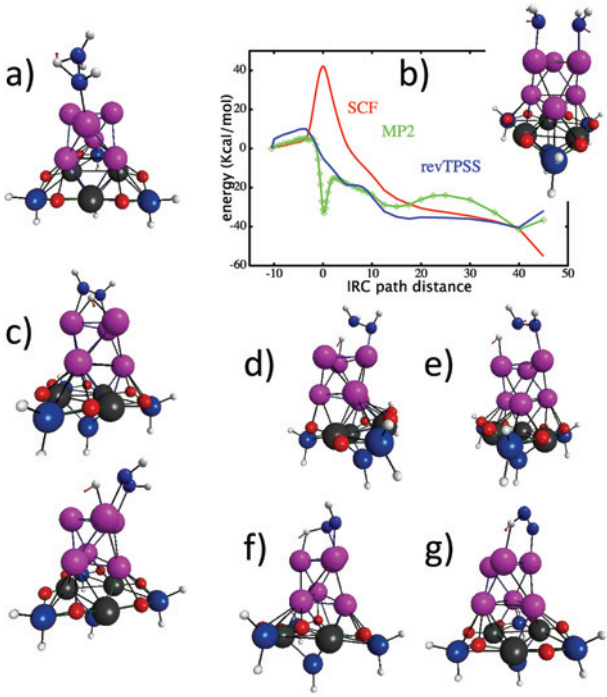

Fig. 7. NN and NH bond breaking saddle point structures: a) isomerization of hydrazine to activated hydrazine. b) NN cleavage to $2NH_2$ (see text). c) NH cleavage in N_2H_4 across two Ir atoms, or just one. d) NH cleavage across 2 Ir atoms for activated hydrazine. e) NH cleavage across 2 Ir atoms for N_2H_3. f) and g) are NH cleavages for HNNH and NNH, respectively. Atom color code as in Fig. 4.

4D. N_2H_4 and H_3NNH adsorption. Hydrazine adsorption can occur at an upper corner of the Ir cluster, with a single N→Ir lone pair interaction, with an interaction energy of −32(−37) kcal/mol. However, two such N→Ir interactions producing a roughly rectangular geometry has a similar interaction energy, −43(−38) kcal/mol, with only a small barrier separating these two isomers. The double coordination arrangement for hydrazine is shown in Fig. 6. Thus hydrazine surface species are coordinated to one or two Ir atoms. Interestingly, adsorbed "activated hydrazine" H_3NNH is singly coordinated through its NH end, and lies at a much higher energy of −6(− 14) kcal/mol. The isomerization barrier separating doubly coordinated hydrazine from activated hydrazine occurs at an overall energy of +27(+20) kcal/mol: the direct barrier from −43(−38) to +27(+20) = 70(58) kcal/mol is almost unchanged from the 63 kcal/mol isomerization barrier in the gas phase. This isomerization saddle point structure is illustrated in Fig. 7.

4E. Other adsorbed species. Figure 6 shows typical structures for adsorbed N_xH_y species. The structures shown are not necessarily the lowest energy isomers for each, as a few cases are chosen to illustrate the possibility of coordination at the side (HNNH), or distortion in the catalyst model (^{1}NH bonding to an Ir_3 face, or $^2NH_2$). The adsorp-

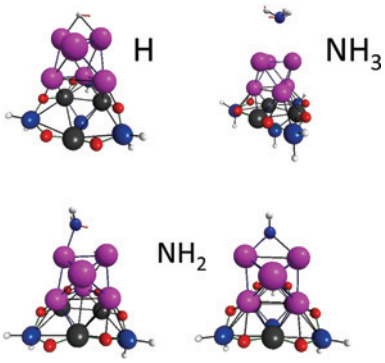

Fig. 8. Ir to Ir site hopping mechanisms for H, NH_3, and NH_2. For the latter, SCF calculations give a bridged intermediate (lower right), with mirror image saddle point structures (lower left) connecting equivalent vertical isomers to the bridged intermediate. MP2 calculations reverse the energy ordering, making the bridged species barely higher than the saddle. See text for energies. Atom color code as in Fig. 4.

tion energies for the most stable isomers are also given in Fig. 6. The most stable isomer usually has the adsorbate above the top Ir_3, an undistorted octahedron, and all six IrO connections to the alumina model. Note that in this figure, energies are not shifted to the 2N/4H energy scale, but rather are the direct adsorption energies: $N_xH_y(g) + Ir_6/\text{model} \rightarrow N_xH_y/Ir_6/\text{model}$. The adsorption energies for singlet H + H on either a single Ir or on two adjacent Ir atoms are measured relative to $H_2(g) + Ir_6/\text{model}$. The energies of adsorption are all fairly large, even for N_2, so this is chemisorption. A physisorbed $H_2/Ir_6/\text{model}$ with very long IrH distances (not shown) was the only species found which was not chemisorbed.

4F. Site hopping. If dissociation creates species like H or NH_2 on the surface, these may hop from site to site on larger Ir particles, and then possibly recombine to form products like H_2 or NH_3. It is therefore interesting to consider the barriers to hopping for H, NH_2, and NH_3. H atoms migrate through a saddle, shown in Fig. 8 with slightly asymmetrical IrH distances. This saddle point connects two inequivalent isomers, both with H atoms above an Ir, differing by 9 kcal/mol. The direct hopping barrier is 7 kcal/mol above the higher energy isomer, so H motion across the surface should be facile. The H-atom hopping barrier predicted here is somewhat larger than the 2 kcal/mol value found in a DFT plane wave study of H-atom coverage of the Ir(111) surface [108]. The hopping of NH_2 is more complicated. The SCF pathway is symmetric, with two equivalent minima for NH_2 located above a single Ir (see Fig. 6). The SCF pathway also has a bridged minimum, with the NH_2 inserted into the IrIr top edge, 2 kcal/mol below these equivalent minima. A skewed triangular transition state lying 6 kcal/mol above the two equivalent minima connects these with the bridged minima (this saddle and the bridged minima are shown in Fig. 8). Adding correlation energy via MP2 makes the bridged minimum the high point on the reaction path, lying 2 kcal/mol above the equivalent NH_2 minima, with the original transition state lying only 0.2 kcal/mol lower than the bridged geometry. Surface migration of NH_2 is thus even more facile than H atom migration, requiring only about 2 (*vs.* 7) kcal/mol. The migration of adsorbed NH_3 proceeds through

a nearly desorbed saddle point shown in Fig. 8, whose direct barrier of 17 kcal/mol is more than half the 28 kcal/mol adsorption energy for the NH_3/Ir_6/model.

4G. NN cleavage. The saddle point structure for breaking the NN bond on the closed shell singlet surface is shown in Fig. 7 and is unremarkable. Following the reaction path forward leads to two NH_2 groups attached to adjacent Ir atoms, with one NH_2 above the attached Ir, and the other pointing out sideways, with the attached N nearly in the same plane as the three top Ir atoms (not shown). The MP2 energy at the SCF saddle point is rather low. So, the energy profile for NN cleavage was evaluated along the entire IRC at the MP2 and DFT levels of theory (using the revTPSS functional [109]), as shown in Fig. 7, and also by single point CCSD(T) energies at the SCF saddle point. The DFT energy profile shows a direct barrier which is shifted towards the reactants, of about 10 kcal/mol, so that at the SCF saddle point, the DFT energy lies below the reactants. Direct energies for CCSD and CCSD(T) at the SCF saddle point geometry lie +6 and −3 kcal/mol above adsorbed N_2H_4. The NN cleavage is thus facile, occurring at an overall energy of about −33 kcal/mol, if the direct barrier is taken to be ≤10 kcal/mol. This ≤10 kcal/mol direct barrier is remarkably reduced from the gas phase NN bond dissociation energy of about 65 kcal/mol! The catalyzed cleavage of the NN bond is due to the aforementioned ability of the Ir cluster to stabilize surface radicals, and singlet states. The low barrier found for NN cleavage also supports the experimentally proposed initiation step on Shell 405 [1,101].

4H. NH cleavage. Direct dissociation of an NH bond in hydrazine occurs in two ways, with both saddle point structures illustrated in Fig. 7. One of these saddle points leaves the H atom on the same Ir that is also coordinated to the NH end of N_2H_3. The other saddle point transfers the H atom directly to an adjacent Ir atom (the bare Ir atom in the reacting N_2H_4/Ir_6/model). These two NH cleavages have very similar overall energy requirements: −15(−8) kcal/mol for single site cleavage, compared to +8(−5) kcal/mol for the two site cleavage, so both lie just below the energy of the reactant $N_2H_4(g) + Ir_6$/model. The reaction path leading away from the single center saddle point contains additional rearrangements (not illustrated) with lower energies for all subsequent steps: an intermediate where H and the NH end of N_2H_3 are bound to the same Ir atom, at energy −18(−31) kcal/mol, a H-bridged intermediate at −3(−30) kcal/mol, and finally reaching separated H + doubly coordinated N_2H_3 at −16(−29) kcal/mol, in which all three Ir sites are occupied. For this slightly lower energy single site cleavage, the direct barrier for NH scission starting from the initial doubly coordinated N_2H_4/Ir_6/model (whose energy is −43(−38) kcal/mol) is just 28(30) kcal/mol; this is significantly reduced from the gas phase NH bond dissociation energy of 81 kcal/mol.

Figure 7 also shows the NH cleavage in "activated hydrazine", which is adsorbed only weakly, causing the barrier height to be small, −8 kcal/mol at the CCSD(T) level. (This particular saddle point structure has a large T_1 diagnostic [110], so the corresponding MP2 barrier of +34 kcal/mol is less reliable). The reaction path beyond this saddle point, whose direct barrier is just +6 kcal/mol, leads to a product with H_2NNH doubly coordinated at the side of the Ir_6 cluster, rather than at the top, and with the dissociated H atom above the same Ir that binds the H_2N end of H_2NNH. This 6 kcal/mol

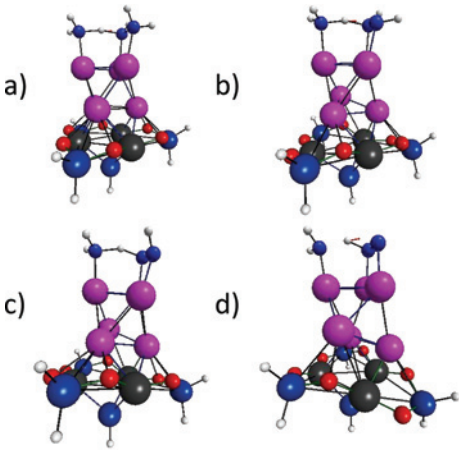

Fig. 9. Frames a through d show the saddle point for NH_2 abstraction of hydrogen from N_2H_4, N_2H_3, N_2H_2, and NNH, respectively. The product NH_3 remains absorbed on the leftmost Iridium atom. Atom color code as in Fig. 4.

CCSD(T) direct barrier is lower than the 28(30) kcal/mol direct barrier for single Ir site NH cleavage in hydrazine given above, but recall that there is a +27(+20) kcal/mol isomerization overall energy requirement to produce activated hydrazine (section 4D). Thus NH cleavages occur from normal hydrazine with the lower overall energy requirements of −8 and −5 kcal/mol discussed in the previous paragraph.

NH cleavage in the radical N_2H_3 is more straightforward: The doubly coordinated adsorption minimum of N_2H_3, shown in Fig. 6, is at −46 kcal/mol, similar to the −43 kcal/mol energy of adsorbed hydrazine. The saddle point structure shown in Fig. 7 corresponds to a direct transfer of H to a bare top Ir atom, with the reaction path leading without any intermediate steps to H plus singly coordinated cis-HN=NH. The direct barrier for this is +34 kcal/mol, slightly smaller than the abstraction of this H by an NH_2 (see below). The adsorbed products H + *cis*-HNNH lie 18 kcal/mol above adsorbed N_2H_3. The saddle point lies 12 kcal/mol below N_2H_3(g) + the catalyst model.

4I. H abstraction by NH_2. An alternative way to break NH bonds, to form the observed product NH_3, is to posit that after facile NN cleavage of hydrazine produces $2NH_2$, these NH_2 radicals can abstract H atoms from hydrazine. The energy barrier to hopping by NH_2 was discussed in Sect. 4F, and is moderate. NH_2 species approaching N_2H_y species react through saddle points which have nitrogens bound at all three top Ir sites in the model catalyst, see Fig. 9. The direct MP2 barriers to H-atom abstractions are −1 kcal/mol from N_2H_4, +39 kcal/mol from N_2H_3, +43 kcal/mol from *cis*-HNNH, and +66 kcal/mol from NNH. The direct barrier for the first of these abstractions is 8 kcal/mol at the SCF level, with this saddle point falling slightly below the reactants after MP2 energy correction, so NH_2 abstraction from hydrazine is clearly competitive with the most facile NH bond breaking mechanism discussed above in Sect. 4H. The direct barrier for the H abstraction from N_2H_3, +39 kcal/mol, is slightly higher than the

direct NH cleavage barrier height in N_2H_3 given in Sect. 4H (+34 kcal/mol). Three of the four consecutive abstractions are exothermic, with direct MP2 reaction energies of −8 kcal/mol for NH_3+ N_2H_3, +38 kcal/mol for NH_3+ *cis*-HNNH, −21 kcal/mol for NH_3+ NNH, and −27 kcal/mol for NH_3+ N_2. In this paragraph, the direct barriers and overall energies are reported relative to an energy of zero for each reacting NH_2+ N_2H_y case. The result of two NN cleavages followed by four H-abstractions consumes three N_2H_4 molecules and produces $4NH_3$ molecules, one N_2 molecule and no H_2 molecules, which is exactly the observed low temperature channel [101]. The earlier DFT study of hydrazine on Ir(111) [105] produced results similar to these, except that all four direct NH_2 abstractions were reported to be exothermic. Those workers also found that the required initiating NN cleavage has a slightly higher energy requirement than the first NH cleavage by NH_2 abstraction, as is found here, and that the abstraction barriers go up as each additional H is removed.

It is useful to put the four consecutive abstraction reactions by NH_2 onto a common energy scale. This can be done in the following manner, using two catalyst models to provide as many as 6 Ir sites for N-coordination, so that the energy scale has a total atom count of $6N/12H + 2Ir_6$/model. The transformation processes that connect minima are shown with greater indentation than for the potential energy surface minima:

$2Ir_6$/model + $3N_2H_4$(g)	0.0 kcal/mol
adsorption of three N_2H_4, 1st NN cleavage, and hopping	
2($NH_2/N_2H_4/Ir_6$/model)	−139.5
saddle for 1st abstraction by NH_2	−140.5 (Fig. 9)
$NH_3/N_2H_3/Ir_6$/model + $NH_2/N_2H_4/Ir_6$/model	−148.0
desorption of NH_3, and hopping	
$NH_2/N_2H_3/Ir_6$/model + N_2H_4/Ir_6/model + NH_3(g)	−122.8
saddle for 2nd abstraction by NH_2	−84.2 (Fig. 9)
NH_3/HNNH/Ir_6/model + N_2H_4/Ir_6/model + NH_3(g)	−84.7
desorption of NH_3, 2nd NN cleavage, and hopping	
NH_2/HNNH/Ir_6/model + NH_2/Ir_6/model + $2NH_3$(g)	−86.4
saddle for 3rd abstraction by NH_2	−43.1 (Fig. 9)
NH_3/NNH/Ir_6/model + NH_2/Ir_6/model + $2NH_3$(g)	−107.8
desorption of NH_3, and hopping	
NH_2/NNH/Ir_6/model + Ir_6/model + $3NH_3$(g)	−115.4
saddle for 4th abstraction by NH_2	−48.9 (Fig. 9)
$NH_3/N_2/Ir_6$/model + Ir_6/model + $3NH_3$(g)	−142.0
desorption of NH_3 and N_2	
$2Ir_6$/model + N_2(g) + $4NH_3$(g)	−108.8

Many of the species above are radicals, so CCSD(T) calculations could not be performed with GAMESS, and thus only MP2 energy values are given. The overall MP2 energy difference of − 108.8 kcal/mol may be compared to the more accurate coupled-cluster large basis gas phase result of Sect. 2, which is −105.7 (−94.3) kcal/mol without (with) zero point corrections.

All steps are seen to proceed below the energy of reactants. Recall from Sections 4D and 4E that adsorptions and desorptions have no barriers, from section 4G

that NN cleavage of an isolated hydrazine has a direct barrier $\leq$10 kcal/mol and is exothermic, and from Sect. 4F that hopping of an isolated NH_2 from Ir to Ir has a direct barrier of about 2 kcal/mol. The transformations above that lack definitive energies are not expected to have significant energy requirements. Several of the middle steps would have even lower energies if the NH_3 desorptions were postponed. Since the actual catalyst will have many more than six sites, the NH_3 desorptions could easily be slowed while the reacting species "searched" for an active site.

The results presented in this subsection provide a rationale for the low temperature product channel, $4NH_3 + N_2$. The observed reaction at higher temperatures produces $2H_2$ products, as well as N_2, and may involve molecular processes, particularly for the elimination of the last two hydrogens, as well as radical reactions. The high temperature reaction is considered in the next few subsections.

4J. Molecular eliminations. Substantial amounts of H_2 and N_2 are produced during high temperature hydrazine decomposition, in addition to the ammonia found at lower temperatures. The initiating NN cleavage to form NH_2 followed by H atom abstractions can (after four abstractions) explain some N_2 but not H_2 (Sect. 4I). Molecular chemistry offers a possible rationale for both H_2 and N_2 products. For example, two consecutive 1,1- or two consecutive 1,2-H_2 eliminations would generate the high temperature channel $2H_2 + N_2$. No saddle point for 1,2-H_2 elimination from adsorbed hydrazine could be found, but saddle points for consecutive 1,1-eliminations are shown in Fig. 10. The first two hydrogens are eliminated from the nitrogen that remains coordinated to Ir. The energy requirements are quite high, with the first saddle point lying at +55(+48) kcal/mol and the second at +77(+67) kcal/mol, relative to the overall energy zero ($N_2H_4(g) + Ir_6$/model). The overall energy for the first intermediate $H_2(g) + H_2NN/Ir_6$/model is +5(−8) kcal/mol, and for the second intermediate $2H_2(g) + N_2/Ir_6$/model the energy is −33(−34) kcal/mol. The direct barrier for the first elimination, from adsorbed hydrazine, is +87(+84) kcal/mol, and the direct barrier for the second elimination is +72(+75) kcal/mol. These are slightly larger than the gas phase direct barriers of 76 and 52 kcal/mol, so the catalyst is not favorably modifying either 1,1-H_2 elimination.

Alternatively, six-center saddle point structures can be considered, by allowing H_2, NH_3, or N_2H_4 from the gas phase to assist two consecutive 1,2-H_2 eliminations. Figure 10 shows two of the six saddle points that were found, namely for H_2 assisting the first 1,2-H_2 elimination, and for unreacted hydrazine assisting the second. The assisted barriers remain large, and similar to those found for the gas phase processes. For the first H_2 assisted elimination the direct barrier is 75(85) kcal/mol, compared to 69 kcal/mol in the gas phase. For the second N_2H_4 assisted elimination, the direct barrier is 60(58) kcal/mol, compared to 76 kcal/mol in the gas phase. Once again, the catalyst is not modifying the barriers for molecular chemistry. Overall, the 2N/4H scale MP2-level energy requirements for H_2 assistance for the first and second 1,2-H_2 eliminations are +34 and +39 kcal/mol, respectively. For NH_3 assistance, the overall energy requirements at the two saddles are +20 and +35 kcal/mol. For hydrazine assistance, the overall energy requirements are +18 and +32 kcal/mol.

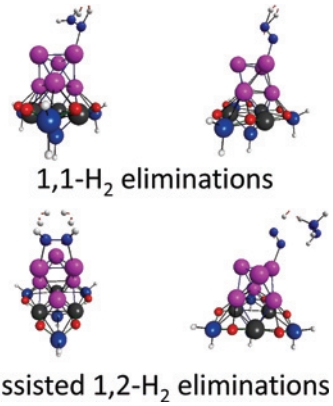

Fig. 10. Top row shows the first and second 1,1-H_2 eliminations to produce adsorbed N_2. Bottom row shows lower energy pathways, where the assisting gaseous H_2 or the NH bond of another hydrazine creates 6-center transition states. Atom color code as in Fig. 4.

An overall summary, in which the assisting species for both dehydrogenations, labeled (a), is chosen to be N_2H_4, follows. Once again, transformation steps between minima are shown with greater indentation than are the lines for minima:

$N_2H_4(a) + N_2H_4(g) + Ir_6/model$	0.0 kcal/mol
adsorption of hydrazine	
$N_2H_4(a) + N_2H_4/Ir_6/model$	−42.5
saddle for assisted 1,2-H_2 elimination	17.6
$N_2H_4(a) + H_2(g) + cis\text{-}HNNH/Ir_6/model$	−21.0
saddle for assisted 1,2-H_2 elimination	32.2 (Fig. 10)
$N_2H_4(a) + 2H_2(g) + N_2/Ir_6/model$	−33.2
desorption of N_2	
$N_2H_4(a) + 2H_2(g) + N_2(g) + Ir_6/model$	−17.2

As noted just above, similar overall saddle point energetics pertain if the assisting species is instead either H_2 or NH_3. The overall MP2 exothermicity of 17.2 kcal/mol can be compared to the more accurate large basis set coupled-cluster gas phase results given above, which is 8.3 (9.4) kcal/mol without (with) zero point energy corrections. The positive energies at the assisted elimination saddle points mean that higher temperatures would be required for this mechanism than for the lower energy NH_2 abstraction pathway discussed in Sect. 4I.

4K. H_2 and N_2 production. Molecular routes leading to H_2 and N_2 were just discussed, occurring at approximately 30 kcal/mol above hydrazine + catalyst.

Since H hopping is facile, an additional source of H_2 product could be H + H recombination on the surface. The final details in H + H recombination are shown in Fig. 11. The recombination occurs by bringing two H atoms to the same Ir atom, where they can pass over a saddle point to produce chemisorbed H_2, prior to desorption. The direct MP2 barrier for the reverse, namely splitting the chemisorbed H_2 is +9 kcal/mol,

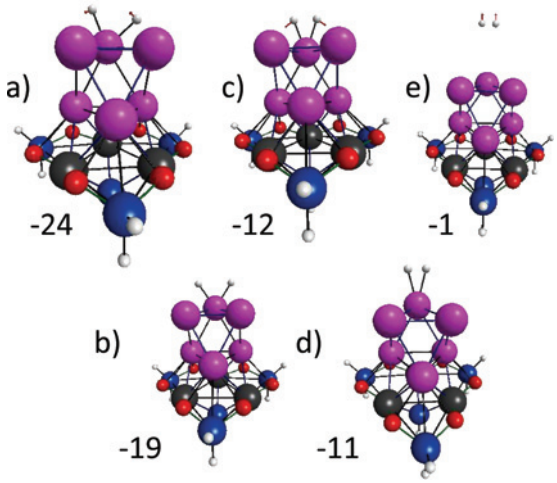

Fig. 11. Frames a, c, and e are saddle points showing how a bridged/capped minimum (not shown) leads to minimum b with two H atoms on the same Iridium, to minimum d with a chemisorbed H_2 on one Iridium, and to its desorption to the gas phase. Energies are CCSD(T) values, relative to $H_2(g) + Ir_6$/model at 0.0 kcal/mol. Atom color code as in Fig. 4.

and essentially disappears (−1 kcal/mol) at the CCSD(T) level of theory. Energies on a scale with the zero set to $H_2(g) + Ir_6$/model are given in Fig. 11, and show that hopping to a common atom to then recombine is facile. The formation of H_2 on a single corner atom is reminiscent of the first NH_3 formation reaction that will be discussed in Sect. 4L, and also the first NH cleavage reaction discussed in Sect. 4H. The presence of reactive corner atoms offers a hypothesis for why the supported nanoparticles in Shell 405 are more effective than the Ir(111) surface at hydrazine decomposition.

Since H_2 can be formed by recombination, it is important to consider the successive NH cleavages of hydrazine to create the required H atoms. The NH cleavage in hydrazine or activated hydrazine, and the second NH cleavage in N_2H_3, which produce surface H atoms, was discussed in Sect. 4H. These first two NH scissions occur at lower overall energy requirements than for assisted 1,2-H_2 eliminations at ≈ +32–39 kcal/mol (Sect. 4J); namely −8 kcal/mol for N_2H_4 and 20 kcal/mol for H_3NNH (relative to $N_2H_4 + Ir_6$/model) according to CCSD(T), and −12 kcal/mol for H_2NNH radical (relative to $N_2H_3 + Ir_6$/model), according to MP2. After two NH bonds are broken, the geometry for doubly coordinated *cis*-HNNH has both hydrogens pointing outwards, away from the plane of the three Ir atoms, far from the adjacent Ir atom. The saddle points for the third and fourth NH cleavages are shown in Figs. 7f and 7g, and the HNNH torsion in the former is seen to be a highly strained 90°. This causes a relatively high barrier for the third NH scission, namely +47(+37) kcal/mole above $N_2H_4 + Ir_6$/model, which is slightly higher than the second assisted 1,2-H_2 elimination at ≈ +32–39 kcal/mol. An additional reason for thinking that the assisted molecular routes, particularly for removal of the third and fourth hydrogens, are competitive is that these mechanisms involve fewer total steps, and the assisting species are likely to possess high kinetic energy in the decomposition flame.

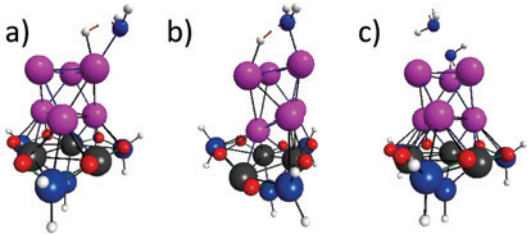

Fig. 12. Transition states producing ammonia: a) H + NH_2 recombination occurring on a single Ir atom, b) recombination occurring from adjacent Ir atoms, c) NH_3 release from activated hydrazine. Atom color code as in Fig. 4.

N_2 is produced by both the low temperature route (four consecutive NH_2 abstractions of H atoms), and both alternatives for the high temperature route (assisted 1,2-H_2 eliminations, or loss of H atoms from N_xH_y to the surface, both leaving behind adsorbed N_2).

4L. NH_3 production. Abstraction routes to the observed ammonia product were discussed in Sect. 4I: following hydrazine NN bond cleavage, the NH_2 can readily abstract an H atom from another hydrazine or less readily, from N_2H_y.

An alternative to abstraction by NH_2 involves surface diffusion of H atoms to sites adjacent to NH_2, prior to recombination as NH_3 [101]. Two modest energy saddles for recombination were found (see Figs. 12a and 12b). The saddle point 12a involves NH bond formation between H and NH_2 located on the same Ir atom, necessitating first a hop of H from an adjacent Ir. The reaction mechanism begins with an H atom directly above an Ir site (vertical orientation), and an NH_2 group at an adjacent Ir, oriented with the N in the same plane as the three Ir atoms (sideways coordination). By several steps (not shown) passing through two lower energy saddle points and two different H-bridging minima, the reaction arrives at the true bottleneck for single site recombination, namely structure 12a. 12a has the highest energy during the recombination, at +13(+6) kcal/mol above dissociated NH_3+ Ir_6/model, meaning that the barrier for the reverse reaction, namely a direct barrier for NH cleavage for NH_3/Ir_6/model on a single Ir atom, is +41(+40) kcal/mol. This may be compared to the direct NH cleavage energy for N_2H_4 on a single Ir site of +28(+30) kcal/mol (see Sect. 4H).

The second recombination MP2 saddle point shown in Fig. 12b also lies 13 kcal/mol above dissociated NH_3+ Ir_6/model. In its reverse direction, this recombination saddle point corresponds to a direct dissociation of ammonia to H and NH_2 on adjacent centers (no bridging intermediates). The reaction path for the two Ir site recombination is connected to a quite distorted NH_3/Ir_6/model with open top/bottom Ir edges, and an adsorption energy of only 23, rather than 28, kcal/mol (Fig. 6). The direct NH cleavage energy from this distorted species requires 36 kcal/mol, which may be compared to the value of 51 kcal/mol for the two-site NH scission of N_2H_4 (see Sect. 4H). The values in this paragraph are all MP2 energies, since CCSD iterations did not converge for 12b, which has a rather distorted Ir_6 moiety.

A final saddle point which generates NH_3 product is shown in Fig. 12c. This saddle point involves NN cleavage in "activated hydrazine", to generate a surface NH

species. The direct MP2 barrier for NH_3 dissociation from the adsorbed H_3NNH is only 9 kcal/mol, and essentially disappears (−3 kcal/mol) at the CCSD(T) level of theory. However, recall that the H-atom migration to produce adsorbed activated hydrazine mentioned in Sect. 4H is at an overall energy of +27(+20) kcal/mol, so this isomerization is the true bottleneck, rather than the NN cleavage.

Thus the major source of ammonia is predicted to involve NN cleavage in adsorbed hydrazine, giving adsorbed surface NH_2 species, followed by H atom abstractions from N_2H_y. Recombination of $H + NH_2$ is a minor source, while loss of ammonia from activated hydrazine is even less important.

5. Summary

The gas phase decomposition of hydrazine has been carefully reexamined using advanced electronic structure methods, with reasonable basis sets. Radical mechanisms and alternative molecular mechanisms are found to be competitive in the energy interval about 65 to 81 kcal/mol above hydrazine, corresponding to its experimental NN and NH bond strengths. Activated hydrazine appears to be a minor player in the gas phase, as an assisted isomerization to produce it, and a reaction with H_2 to produce ammonia lies just above the lowest energy radical pathway, namely NN cleavage. By definition, the saddle points presented in Table 1 are elementary reactions, and differ considerably from those used in the current best kinetics model of Konnov and J. de Ruyck [5]. The new set of reactions and barrier height data might hopefully serve as a basis for a revised kinetics model for the gas phase decomposition.

Calculations on α-alumina slabs showed that there is substantial chemical interaction between iridium and the alumina surface, requiring very large slabs to make a rigid model, which inspired the development of the much more tractably sized Si-containing model.

A fairly realistic molecular model for the Shell 405 catalyst was created by mounting an Ir_6 octahedron on a bottom tethered c-[-O-AlH-SiH_2-]$_3$SiH ring, so that each of the three bottom Ir atoms has two direct IrO and one direct IrAl contacts. These Ir atoms are not close to the ring Si atoms, or to the final Si atom tethering the 12-atom ring from below. Both types of silicon impart rigidity to the Ir_6/model. A number of calculations with an Ir_4 tetrahedron show that the corresponding Ir_4/model is much more deformable under attack by N_xH_y species than is the octahedron of the Ir_6/model. Another advantage of Ir_6 compared to Ir_4 is an increased number of top Ir sites where reactants can coordinate. This is very likely the explanation for the general experimental trend that Ir_x activity increases with particle size. The Ir_6/model allows coordination at the side as well as at the top, has IrIr edges where insertion may happen, and contains reactive corner atoms where single bonds can break. All of these possibilities occur, but none are possible if the catalyst is the Ir(111) surface. The Ir_6/model is small enough to allow the use of double-zeta polarized basis sets with MP2 and some CCSD(T) energy corrections, so the accuracy for the energies of hydrazine decomposition on the model catalyst is less than the very accurate gas phase results.

In agreement with conventional wisdom [1,101], and an earlier theoretical study of hydrazine decomposition on Ir(111) [105], the lowest energy pathway involves NN

cleavage (direct barrier $\leq$10 kcal/mol) to produce surface NH_2, which abstracts four H atoms sequentially from N_2H_y, going all the way to N_2. The first such abstraction is essentially barrierless, and the remaining three abstractions have saddle point energies below that of the gas phase reactants. The initial direct NN cleavage barrier is dramatically altered from the 65 kcal/mol bond energies in the gas phase, no doubt due to the ability of the catalyst to quench surface radical character. Stepwise H-atom abstractions by four NH_2 radicals nicely explains the low temperature channel, $3N_2H_4 \rightarrow 4NH_3 + N_2$.

The higher temperature channel $N_2H_4 \rightarrow N_2 + 2H_2$ is more ambiguous. The initial two NH cleavages first from hydrazine and then from N_2H_3 to produce surface H atoms are found to have overall barriers that are slightly below the gas phase reactants: the first NH cleavage is at -8 kcal/mol relative to the reactants $N_2H_4(g) + Ir_6$/model. Four such NH cleavages could produce two H_2 from two H + H recombinations on the surface, leaving behind N_2 to also desorb. This has been suggested previously on the Ir(111) surface [105], but the number of dissociation steps, hops, and recombinations required is large. A shorter molecular route through assisted 6-center saddle points is proposed here, and found to lie $\approx$30 kcal/mol above the gas phase reactant + catalyst. These two processes may well compete in the high temperature limit, and they are not mutually exclusive. The first two hydrogens are definitely more easily removed from hydrazine by NH cleavage to surface H atoms, followed by H + H recombination. The final two hydrogens in adsorbed *cis*-HNNH are directed outwards, directly away from the surface, meaning their removal by assisted molecular saddle points is competitive with radical cleavage of the final two hydrogens.

After hypergolic ignition of the hydrazine flame by the catalyzed surface reactions, the overall exothermicity of these surface reactions means that the flame will contain hot product molecules. Collisions in the gas phase above the catalyst will then occur at higher energies, meaning that the gas phase reactions described in Sect. 2 are likely to begin. The hydrazine thruster is simple from an engineering viewpoint, but the network of decomposition reactions of hydrazine in this thruster appears to be remarkably complex.

The chemistry that can occur on the Ir_6/model catalyst is extensive. For example, one mechanism to produce ammonia is a recombination of surface $H + NH_2$ species that can occur at corner atoms. Radicals such as H and NH_2 sometimes insert into IrIr bonds, which may poison the catalyst, if these remain inserted. Ir_6 distortions occur, particularly lengthening of the IrO contacts when radicals are adsorbed, and transfer their radical character into the Ir cluster atoms. The catalyst is remarkably effective in lowering initial radical formation compared to the gas phase bond energies, for both the initiating NN cleavage as well as various NH cleavages. There are also low energy requirements for abstractions from N_2H_y by NH_2. On the other hand, the catalyst has little effect on direct barrier heights for molecular reactions, such as assisted or unassisted H_2 eliminations. Activated hydrazine does not seem to be an important species on the catalyst, because the catalyst does not stabilize the isomerization reaction needed to generate absorbed H_3NNH. If formed, however, activated hydrazine readily loses NH_3 and has a low energy first NH cleavage.

It is reasonable to speculate on the relevance of reactions on the present Ir_6/model catalyst to hydrazine decomposition on 2 nm sized Shell 405 Ir particles. The quench-

ing of radical character in surface species by the small Ir_6/model is likely to be enhanced for larger metal particles. Shell 405 particles presumably also have flat regions with hexagonally arranged Ir_3 triangles (akin to the Ir(111) surface), instead of just one top triangle in Ir_6/model. On the other hand, the larger particle will have relatively fewer corner atoms and edges, which may be more reactive than hexagonal regions.

Acknowledgement

The research presented here is based upon work supported by the Air Force Office of Scientific Research under AFOSR Award No. FA9550-09-1-0059. The calculations were performed under the auspices of a Department of Defense Grand Challenge grant of computer time, on a computer cluster that was purchased in part by a DoD DURIP grant, and on a GPU-based cluster that was provided in part by the Nvidia Corporation, the Ames Laboratory, and Iowa State University. The authors are very grateful to Dr. Spencer Pruitt for many helpful discussions.

References

1. E. W. Schmidt (Ed.), Hydrazine and its Derivatives, 2nd edition, 2 volumes, Wiley Interscience, New York (2001).
2. W. E. Armstrong, L. B. Ryland, and H. H. Voge, US Patent 4124538 (1978) (Chem.Abstracts 90, 444504).
3. K. W. Michel and H. Gg. Wagner, 10th Symp. on Combustion (1965) 353.
4. D. D. Wagman, W. H. Evans, V. B. Parker, R. H. Schumm, I. Halow, S. M. Bailey, K. L. Churney, and R. L. Nuttall, J. Phys. Chem. Ref. Data 11 (1982) Supplement 2.
5. A. A. Konnov and J. de Ruyck, Combustion and Flame **124** (2001) 106.
6. I. J. Eberstein and I. Glassman, 10th Symp. on Combustion (1965) 365.
7. L. Zhang, A. C. T. van Duin, S. V. Zybin, and W. A. Goddard, J. Phys. Chem. B **113** (2009) 10770.
8. D.-Y. Hwang and A. M. Mebel, J. Phys. Chem. A **107** (2003) 2865.
9. R. Asatryan, J. W. Bozelli, G. da Silva, S. Swinnen, and M. T. Nguyen, J. Phys. Chem. A **114** (2010) 6235.
10. C. M. Aikens, S. P. Webb, R. L. Bell, G. D. Fletcher, M. W. Schmidt, and M. S. Gordon, Theoret. Chem. Acc. **110** (2003) 233.
11. C. M. Aikens, G. D. Fletcher, M. W. Schmidt, and M. S. Gordon, J. Chem. Phys. **124** (2006) 014107.
12. R. A. Kendall, T. H. Dunning, and R. J. Harrison, J. Chem. Phys. **96** (1992) 6796.
13. P. Piecuch and M. Wloch, J. Chem. Phys. **123** (2005) 224105.
14. M. Wloch, J. R. Gour, and P. Piecuch, J. Phys. Chem. A **111** (2007) 11359.
15. P. Piecuch, J. R. Gour, and M. Wloch, Int. J. Quantum Chem. **109** (2009) 3268.
16. M. W. Schmidt and M. S. Gordon, Annu. Rev. Phys. Chem. **49** (1998) 233.
17. H. Nakano, J. Chem. Phys. **99** (1993) 7983.
18. M. W. Schmidt, K. K. Baldridge, J. A. Boatz, S. T. Elbert, M. S. Gordon, J. H. Jensen, S. Koseki, N. Matsunaga, K. A. Nguyen, S. J. Su, T. L. Windus, M. Dupuis, and J. A. Montgomery, J. Comput. Chem. **14** (1993) 1347.
19. M. S. Gordon and M. W. Schmidt in: Theory and Applications of Computational Chemistry, the First Forty Years C. E. Dykstra, G. Frenking, K. S. Kim, and G. E. Scuseria (Eds.), Elsevier, Amsterdam (2005), pp. 1167–1189.
20. H. Biehl and F. Stuhl, J. Chem. Phys. **100** (1994) 141.
21. J. M. L. Martin and P. R. Taylor, Mol. Phys. **96** (1999) 681.

22. B. Ruscic and J. Berkowitz, J. Chem. Phys. **95** (1991) 4378.
23. Although MP2 level saddle points can be located, MCSCF saddles were used for direct 1,2 H_2 eliminations, as this portion of the potential surface is moderately multireference. For example, at the saddle for hydrazine's direct dissociation to *cis* HN=NH, the MCSCF 4e-in 4φ occupation numbers are 1.97, 0.70, 0.30, 0.03. CR-CC(2,3) energies at these MCSCF saddles were used to construct the energy diagrams.
24. W. D. Hinsberg and P. B. Dervan, J. Am. Chem. Soc. **100** (1978) 1608.
25. T.-K. Ha, M. T. Nguyen, and P. Ruelle, Chem. Phys. **87** (1984) 23.
26. The second order saddle point has C_s symmetry, $\omega = 1399$i (a') and 669i(a"), the former being the correct motion for this type of elimination. Searches to eliminate the smaller imaginary frequency resulted in locating a saddle point in C_1 for a different reaction, namely the H_2-assisted isomerization of N_2H_4 to H_3NNH shown in Fig. 2a. The SOSP's energy value is used here only to indicate a relatively high energy for this particular H_2 elimination.
27. This energy is not zero point corrected. The MECP was located by closed and spin-restricted open shell perturbation theory, using the same basis set as for all other saddles. The CR-CC(2,3) energies with the triple zeta basis agree to each other within 3 kcal/mol and the +9 quoted is the average of these two energies.
28. Z.-F. Xu, D.-C. Fang, and X.-Y. Fu, Int. J. Quantum Chem. **70** (1998) 321.
29. N. C. Baird and J. R. Swenson, Can. J. Chem. **51** (1973) 3097.
30. C. J. Casewit and W. A. Goddard, J. Am. Chem. Soc. **102** (1980) 4057.
31. M. W. Schmidt and M. S. Gordon, Inorg. Chem. **25** (1986) 248.
32. G. Schulz-Ekloff and R. Hoppe, Cat. Lett. **6** (1990) 383.
33. T. G. Soares Neto, A. J. G. Cobo, and G. M. Cruz, Appl. Catal. A **250** (2003) 331.
34. S. J. Cho, J. Lee, Y. S. Lee, and D. P. Kim, Catal. Lett. **109** (2006) 181.
35. Y. B. Jang, T. H. Kim, M. H. Sun, J. Lee, and S. J. Cho, Catal. Today **146** (2009) 196.
36. B. J. Wood and H. Wise, J. Catalysis **39** (1975) 471.
37. H. H. Sawin and R. P. Merrill, J. Chem. Phys. **73** (1980) 996.
38. O. I. Smith and W. C. Solomon, Ind. Eng. Chem. Fundam. **21** (1982) 374.
39. G. A.-P. Papapolymerou, A. G. Botis, A. D. Papargyris, X. D. Spiliotis, and D. Kasidakis, React. Kinet. Catal. Lett. **49** (1993) 339.
40. R. Vieira, D. Bastos-Netto, M.-J. Ledoux, and C. Pham-Huu, Appl. Cat. A **279** (2005) 35.
41. Z. Xu, F.-S. Xiao, S. K. Purnell, O. Alexeev, S. Kawi, S. E. Deutsch, and B. C. Gates, Nature **372** (1994) 346.
42. A. M. Argo, J. F. Odzak, F. S. Lai, and B. C. Gates, Nature **415** (2002) 623.
43. S. Kawi, J.-R. Chang, and B. C. Gates, J. Phys. Chem. **97** (1993) 10599.
44. A. Uzun and B. C. Gates, J. Am. Chem. Soc. **131** (2009) 15887.
45. J. Prasad and J. L. Gland, Langmuir **7** (1991) 722.
46. K. M. C. Davis and C. F. Sayer, J. Chem. Soc., Faraday Trans. 1 **68** (1972) 1884.
47. X. Chen, T. Zhang, M. Zheng, Z. Wu, W. Wu, and C. Li, J. Catal. **224** (2004) 473.
48. R. Brayner, G. Djega-Mariadassou, G. Marques da Cruz, and J. A. J. Rodrigues, Catalysis Today **57** (2000) 225.
49. J. Block and G. Schulz-Ekloff, J. Catal. **30** (1973) 327.
50. S. C. Wang and G. Ehrlich, Surf. Sci. **391** (1997) 89.
51. M. R. Churchill and J. P. Hutchinson, Inorg. Chem. **17** (1978) 3528.
52. L. Garlaschelli, S. Martinengo, P. L. Bellon, F. Demartin, M. Manassero, M. Y. Chiang, C.-Y. Wei, and R. Bau, J. Am. Chem. Soc. **106** (1984) 6664.
53. J. Guzman and B. C. Gates, Dalton Trans. (2003) 3303.
54. A. Uzman, D. A. Dixon, and B. C. Gates, Chem. Cat. Chem. **3** (2011) 95.
55. O. Alexeev and B. C. Gates, J. Catal. **176** (1998) 310.
56. A. M. Argo, J. F. Odzik, and B. C. Gates, J. Am. Chem. Soc. **125** (2003) 7107.
57. A. Zhao and B. C. Gates, Langmuir **13** (1997) 4024.
58. F. Li and B. C. Gates, J. Phys. Chem. B **108** (2004) 11259.
59. A. Uzun, V. A. Bhirud, P. W. Kletnieks, J. F. Haw, and B. C. Gates, J. Phys. Chem. C **111** (2007) 15064.
60. A. Uzun and B. C. Gates, Angew. Chem. Int. Ed. **47** (2008) 9245.

61. S. Lee, C. Fan, T. Wu, and S. L. Anderson, J. Phys. Chem. B **109** (2005) 381.
62. C. Fan, T. Wu, W. E. Kaden, and S. L. Anderson, Surf. Sci. **600** (2006) 461.
63. J.-D. Grunwaldt, P. Kappen, L. Basini, and B. S. Clausen, Catal. Lett. **78** (2002) 13.
64. J.-N. Feng, X.-R. Huang, and Z.-S. Li, Chem. Phys. Lett. **276** (1997) 334.
65. J. Du, X. Sun, J. Chen, and G. Jiang, J. Phys. Chem. A **114** (2010) 12825.
66. C. Bussai, S. Kruger, G. N. Vayssilov, and N. Rösch, Phys. Chem. Chem. Phys. **7** (2005) 2656.
67. S. Kruger, C. Bussai, A. Genest, and N. Rösch, Phys. Chem. Chem. Phys. **8** (2006) 3391.
68. M. Trueba and S. P. Trasatti, Eur. J. Inorg. Chem. (2005) 3393.
69. K. Sohlberg, S. T. Pantelides, and S. J. Pennycock, Chem. Eng. Commun. **181** (2000) 107.
70. L. Smrcok, V. Langer, and J. Krestan, Acta Cryst. C **62** (2006) i83.
71. G. Paglia, A. L. Rohl, C. E. Buckley, and J. D. Gale, Phys. Rev. B **71** (2005) 224115.
72. K. Sohlberg, S. T. Pantelides, and S. J. Pennycock, J. Am. Chem. Soc. **123** (2001) 26.
73. F. Maglia, S. Gennari, and V. Buscaglia, J. Am. Ceram. Soc. **91** (2008) 283.
74. A. A. Tsyganenko and P. P. Mardilovich, J. Chem. Soc., Faraday Trans. **92** (1996) 4843.
75. A. Dyan, P. Cenedese, and P. Dubot, J. Phys. Chem. B **110** (2006) 10041.
76. K. Sohlberg, S. T. Pantelides, and S. J. Pennycock, J. Am. Chem. Soc. **121** (1999) 10999.
77. S. Blonski and S. H. Garofalini, Surf. Sci. **295** (1993) 263.
78. S.-D. Mo, Y.-N. Xu, and W. Y. Ching, J. Am. Ceram. Soc. **80** (1997) 1193.
79. A. Ionescu, A. Allouche, J.-P. Aycard, M. Rajzmann, and F. Hutschka, J. Phys. Chem. B **106** (2002) 9359.
80. W. S. Xia, H. L. Wan, and Y. Chen, J. Mol. Catal. A **138** (1999) 185.
81. S.-H. Cai and K. Sohlberg, Recent Res. Devel. Chem. Phys. **3** (2002) 85.
82. L. W. Finger and R. M. Hazen, J. Appl. Phys. **49** (1979) 5823.
83. T. M. French and G. A. Somorjai, J. Phys. Chem. **74** (1970) 2489.
84. B. Hinnemann and E. A. Carter, J. Phys. Chem. C **111** (2007) 7105.
85. H: R. Ditchfield, W. J. Hehre, and J. A. Pople, J. Chem. Phys. **54** (1971) 724.
86. N,O: W. J. Hehre, R. Ditchfield, and J. A. Pople, J. Chem. Phys. **56** (1972) 2257.
87. Al: M. M. Francl, W. J. Pietro, W. J. Hehre, J. S. Binkley, M. S. Gordon, D. J. DeFrees, and J. A. Pople, J. Chem. Phys. **77** (1982) 3654.
88. Si: M. S. Gordon, Chem. Phys. Lett. **76** (1980) 163.
89. W. J. Stevens, M. Krauss, H. Basch, and P. G. Jasien, Can. J. Chem. **70** (1992) 612.
90. K. R. Glaesemann and M. W. Schmidt, J. Phys. Chem. A **114** (2010) 8772.
91. Q. Xu, K. C. Kharas, B. J. Croley, and A. K. Datye, Chem. Cat. Chem **3** (2011) 1004.
92. Q. Xu, K. C. Kharas, B. J. Croley, and A. K. Datye, Topics Catal. **55** (2012) 78.
93. M. Vaarkamp, J. T. Miller, F. S. Modica, and D. C. Koningsberger, J. Catal. **163** (1996) 294.
94. S. N. Rashkeev, K. Sohlberg, M. V. Glazoff, J. Novak, S. J. Pennycook, and S. T. Pantelides, Phys. Rev. B **67** (2003) 115414.
95. A. M. Ferrari, K. M. Neyman, M. Mayer, M. Staufer, B. C. Gates, and N. Rösch, J. Phys. Chem. B **103** (1999) 5311.
96. G. Petrova, G. N. Vayssilov, and N. Rösch, J. Phys. Chem. C **111** (2007) 14484.
97. G. Petrova, G. N. Vayssilov, and N. Rösch, Chem. Phys. Lett. **444** (2007) 215.
98. G. Petrova, G. N. Vayssilov, and N. Rösch, J. Phys. Chem. C **112** (2008) 18572.
99. P. St. Petkov, G. Petrova, G. N. Vayssilov, and N. Rösch, J. Phys. Chem. C **114** (2010) 18572.
100. E. A. Ivanova Shor, V. A. Nasluzov, A. M. Shor, G. N. Vayssilov, and N. Rösch, J. Phys. Chem. C **111** (2007) 12340.
101. J. L. Falconer and H. Wise, J. Catal. **43** (1976) 220.
102. A. E. Makled and H. Belal, 13th International Conference on Aerospace Sciences and Aviation Technology (2009).
103. C. H. Hwang, S. N. Lee, S. W. Baek, C. Y. Han, S. K. Kim, and M. J. Yu, Ind. Eng. Chem. Res. **51** (2012) 5382.
104. H. L. McKay, S. J. Jenkins, and D. J. Wales, J. Phys. Chem. C **115** (2011) 17812.
105. P.-X. Zhang, Y.-G. Wang, Y.-Q. Huang, T. Zhang, G.-S. Wu, and J. Li, Catal. Today **165** (2011) 80.
106. C. Gonzalez and H. B. Schlegel, J. Chem. Phys. **90** (1989) 2154.

107. R. M. Olson, J. L. Bentz, R. A. Kendall, M. W. Schmidt, and M. S. Gordon, J. Comput. Theoret. Chem. **3** (2007) 1312.
108. H. Zhang and W.-X. Li, J. Phys. Chem. C **113** (2009) 21361.
109. J. P. Perdew, A. Ruzsinsky, G. I. Csonka, L. A. Constantin, and J. Sun, Phys. Rev. Lett. **103** (2009) 026403.
110. T. J. Lee and P. R. Taylor, Int. J. Quantum Chem. **S23** (1989) 199.